MUON STOPPING POWER AND RANGE TABLES 10 MeV—100 TeV

DONALD E. GROOM

Ernest Orlando Lawrence Berkeley National Laboratory
1 Cyclotron Road, Berkeley, CA 94556, USA
deg@lbl.gov

and

NIKOLAI V. MOKHOV

Fermi National Accelerator Laboratory
Batavia, IL 60510
mokhov@fnal.gov

and

SERGEI I. STRIGANOV

Fermi National Accelerator Laboratory
Batavia, IL 60510
strigano@fnal.gov
and
IHEP, Protvino, Russia
striganov@mx.ihep.su

The mean stopping power for high-energy muons in matter can be described by $\langle -dE/dx \rangle = a(E) + b(E)E$, where $a(E)$ is the electronic stopping power and $b(E)$ is the energy-scaled contribution from radiative processes—bremsstrahlung, pair production, and photonuclear interactions. $a(E)$ and $b(E)$ are both slowly-varying functions of the muon energy E where radiative effects are important. Tables of these stopping power contributions and continuous-slowing-down-approximation (CSDA) ranges (which neglect multiple scattering and range straggling) are given for a selection of elements, compounds, mixtures, and biological materials for incident kinetic energies in the range 10 MeV to 100 TeV. Tables of the contributions to $b(E)$ are given for the same materials.

Contents

1. Introduction

The mean stopping power for high-energy muons (or other heavy charged particles[1]) in a material can be described by [1]

$$\langle -dE/dx \rangle = a\,(E) + b\,(E)\,E\ , \tag{1}$$

where E is the total energy, $a(E)$ is the electronic stopping power, and $b(E)$ is due to radiative processes—bremsstrahlung, pair production, and photonuclear interactions:

$$b \equiv b_{\rm brems} + b_{\rm pair} + b_{\rm nucl} \tag{2}$$

The notation is convenient because $a(E)$ and $b(E)$ are slowly varying functions of E at the high energies where radiative contributions are important. $b(E)E$ is less than 1% of $a(E)$ for $E \lesssim$ 100 GeV for most materials.

The "continuous-slowing-down-approximation" (CSDA) range is obtained from the integral

$$R\,(E) = \int_{E_0}^{E} \left[a\,(E') + b\,(E')\,E'\right]^{-1} dE' \tag{3}$$

where E_0 is sufficiently small that the result is insensitive to its exact value. At very high energies, where a and b are (essentially) constant,

$$R\,(E) \approx (1/b) \ln\,(1 + E/E_{\mu c}) \quad , \tag{4}$$

where $E_{\mu c} = a/b$ is the muon critical energy. The muon critical energy can be defined more precisely as the energy at which electronic losses and radiative losses are equal, in analogy to one of the ways of defining the critical energy for electrons. It is obtained by finding $E_{\mu c}$ such that

$$a\,(E_{\mu c}) = E_{\mu c} b\,(E_{\mu c}) \quad . \tag{5}$$

The CSDA range is of limited usefulness, particularly at higher energies, because of the effect of fluctuations. (Fluctuations in radiative losses are discussed briefly in Section 4.6.) For example, the cosmic ray muon intensity falls very rapidly with energy, so that the flux observed deep underground is quite different from that to be expected from Eq. (3). We nonetheless calculate the CSDA range given by Eq. (3) as an indicator of actual muon range.

The important and well-studied subjects of stopping power fluctuations and range straggling in electronic energy loss [2,3] are not treated, even though they are much more serious for muons than for heavier particles: The fractional range straggling ($\sqrt{\text{variance(range)}}$/range) scales as $\sqrt{1/M}$ for particles with the same velocity, and hence is three times larger for a 100 MeV muon than for a 900 MeV proton. In copper the fractional straggling varies from 4% at 10 MeV, through a minimum of 2.8% at 300 MeV, then rising through 5.7% at 10 GeV. Above $\sim$ 100 GeV straggling due to fluctuations in bremsstrahlung losses begins to dominate.

Multiple scattering is also neglected, but with more justification. One measure of multiple scattering is provided by the "detour factor" [3], the ratio of the average penetration depth to the average path length for a stopping particle. The detour factor is 0.98 in the worst case (uranium at our lowest energy). This ratio increases rapidly toward unity as the energy is increased or if the atomic weight of the absorber is decreased.

[1] The radiative loss formulae given in this paper apply only to a spin-1/2 pointlike heavy particles, where "heavy" means "much more massive than an electron." Insofar as we know, the solution for spin-0 particles has never been published.

Table 1: Definitions of most of the variables used in this report. The electronic charge e and the kinematic variables $\beta = v/c$ and $\gamma = 1/\sqrt{1-\beta^2}$ have their usual definitions. Constants are from *CODATA Recommended Values of the Fundamental Physical Constants: 1998* [7]. Parenthetical numbers after the values give the 1-standard deviation uncertainties in the last digits. In Sect. 4 the convention $c = 1$ is used.

Symbol	Definition	Units or Value
α	Fine structure constant $e^2/4\pi\epsilon_0\hbar c$	1/137.035 999 76(50)
M	Incident particle mass	MeV/c^2
M_μ	Muon mass	105.658 356 8(52) MeV/c^2
E	Incident particle energy γMc^2	MeV
T	Kinetic energy $(\gamma-1)Mc^2$	MeV
p	Momentum $\gamma\beta Mc$	MeV/c
$m_e c^2$	Electron mass $\times\, c^2$	0.510 998 902(21) MeV
r_e	Classical electron radius $e^2/4\pi\epsilon_0 m_e c^2$	2.817 940 285(31) fm
N_A	Avogadro's number	$6.022\,141\,99(47) \times 10^{23}$ mol^{-1}
ze	Charge of incident particle	
Z	Atomic number of medium	
A	Atomic mass of medium	g mol^{-1}
	(Occasionally: atomic mass number)	dimensionless
K/A	$4\pi N_A r_e^2 m_e c^2/A$ 0.307 075	MeV g^{-1} cm^2 for $A = 1$ g mol^{-1}
I	Mean excitation energy	eV (*Nota bene!*)
δ	Density effect correction to electronic energy loss	
$\hbar\omega_p$	Plasma energy $\sqrt{4\pi N_e r_e^3}\; m_e c^2/\alpha$	$28.816\sqrt{\rho\,\langle Z/A\rangle}$ eV for ρ in g cm^{-3}
N_e	Electron density	
w_j	Fraction by weight of the jth element in a compound or mixture ($\sum w_i = 1$)	
n_j	number of the jth kind of atoms in a compound or mixture	
$E_{\mu c}$	Muon critical energy	GeV
ν	Fractional energy transfer in an incident particle interaction	
ε	νE, the energy transfer in a single interaction	

Tables of muon energy loss from a 1985 CERN internal report by Lohmann, Kopp, and Voss [4] have become the *de facto* world standard. This careful work serves as the benchmark for the present effort. Later theoretical work enables us to improve the calculations for low-Z elements ($2 \le Z \le 10$) and to make minor improvements elsewhere.

It is our intention to make this report sufficiently self-contained that the interested user can replicate our calculations, even though this results in our giving often-tedious detail. The necessary constants for electronic loss calculations and tables of $b(E)$ for elements, for the mean radiative loss calculations, are also available as ASCII files at `http://pdg.lbl.gov/AtomicNuclearProperties`. These tables are more extensive than the subset of data actually presented in this paper.

There is one serious dilemma: We believe that the density effect corrections via the careful parameterizations of Sternheimer et al. [5] are more dependable than those calculated via their general algorithm [6]. But, as will be discussed in Section 3.2, better values for mean excitation energies are now available for a variety of materials. The changes are sometimes as great as 10%. Over much of our energy region of interest (for $\beta\gamma \gtrsim 1000$) however, the density effect has "replaced" the mean excitation energy by the plasma energy, so that improvements in the mean excitation energy have no effect on the stopping power. We therefore continue to use sometimes-obsolete

excitation values. How this affects our results will be discussed in Section 3.2. On the other hand, corrections to the densities used by Sternheimer et al. [5] are easily accommodated if the changes are small; this is done in several cases.

We present tables of stopping power and mean range for muons from kinetic energy $T = 10$ MeV to 100 TeV for most elements and a variety compounds and mixtures. Tables of $b(E)$ are given for the same materials. In the case of elemental gases, tables are also given for the liquid state.

The symbols and constants used in this report are explained in Table 1.

2. Overview

The behavior of stopping power ($= \langle -dE/dx \rangle$) in copper over twelve decades of muon kinetic energy is shown by the solid curves in Fig. 1. Data below the breaks in the curves are from ICRU 49 [3], while data above the breaks are from our present calculations. Approximate boundaries between regions described by different theories or phenomenologies are indicated by the shaded vertical bands. While our main interest is at higher energies, some understanding of the behavior at lower energies is useful, in particular for starting range integrals.

For $\beta < \alpha$, below the first grey band in Fig. 1, the muon velocity is small compared with that of the valence electrons in the absorber. Following the work of Fermi and Teller [9], Lindhard and collaborators have constructed a successful semi-phenomenological model to describe ionizing energy losses in this regime, approximating the electronic structure of solids by a Fermi electron gas distribution [10]. The stopping power is found to be proportional to the projectile velocity. This region is marked by the dashed curve with the dotted extension in Fig. 1. However, below $\beta \approx 0.001$–0.01 nonionizing energy losses via nuclear recoil become increasingly significant [3], finally dominating energy loss at very low energies.

Above $\beta \approx 0.05$ or 0.1 (the second grey band in Fig. 1) one may make the opposite approximation, neglecting electronic motion within atoms. There is no satisfactory theory for the intermediate region, $\alpha < \beta < 0.1$ (but see Ref. 11). There is, however, a rich experimental literature, which Andersen and Ziegler have used to construct phenomenological fits bridging the regions in which there is adequate theoretical understanding [12]. This is the interval between the grey bands shown in Fig. 1.

Electronic (ionization + excitation) losses in the high-velocity region are well described by Bethe's theory based on a first-order Born approximation [13], to which are added a number of corrections for the low-energy region and to account for the polarization of the medium at high energies. The curve falls to a broad minimum whose position for solid absorbers decreases from $\beta\gamma = 3.5$ to 3.0 as Z goes from 7 to 100. The mean electronic loss at the minimum value as a function of Z is shown in Fig. 2. The rise in Fig. 1 with further increases of the projectile energy (labeled "without δ" in Fig. 1) is less marked when the polarization effects are taken into account (dash-dotted curve).

Electronic losses at very high energies are somewhat modified by bremsstrahlung from the atomic electrons [14] (see Section 3.5) and other effects, such as form factor corrections [15]. These are of decreased importance because radiative energy losses begin to be significant above a few hundreds of GeV for even intermediate-Z absorbers. For example, radiative losses in copper dominate above $E_{\mu c} = 315$ GeV. The radiative contribution, and hence the entire energy loss rate, increases nearly linearly with energy above 1 TeV or so.

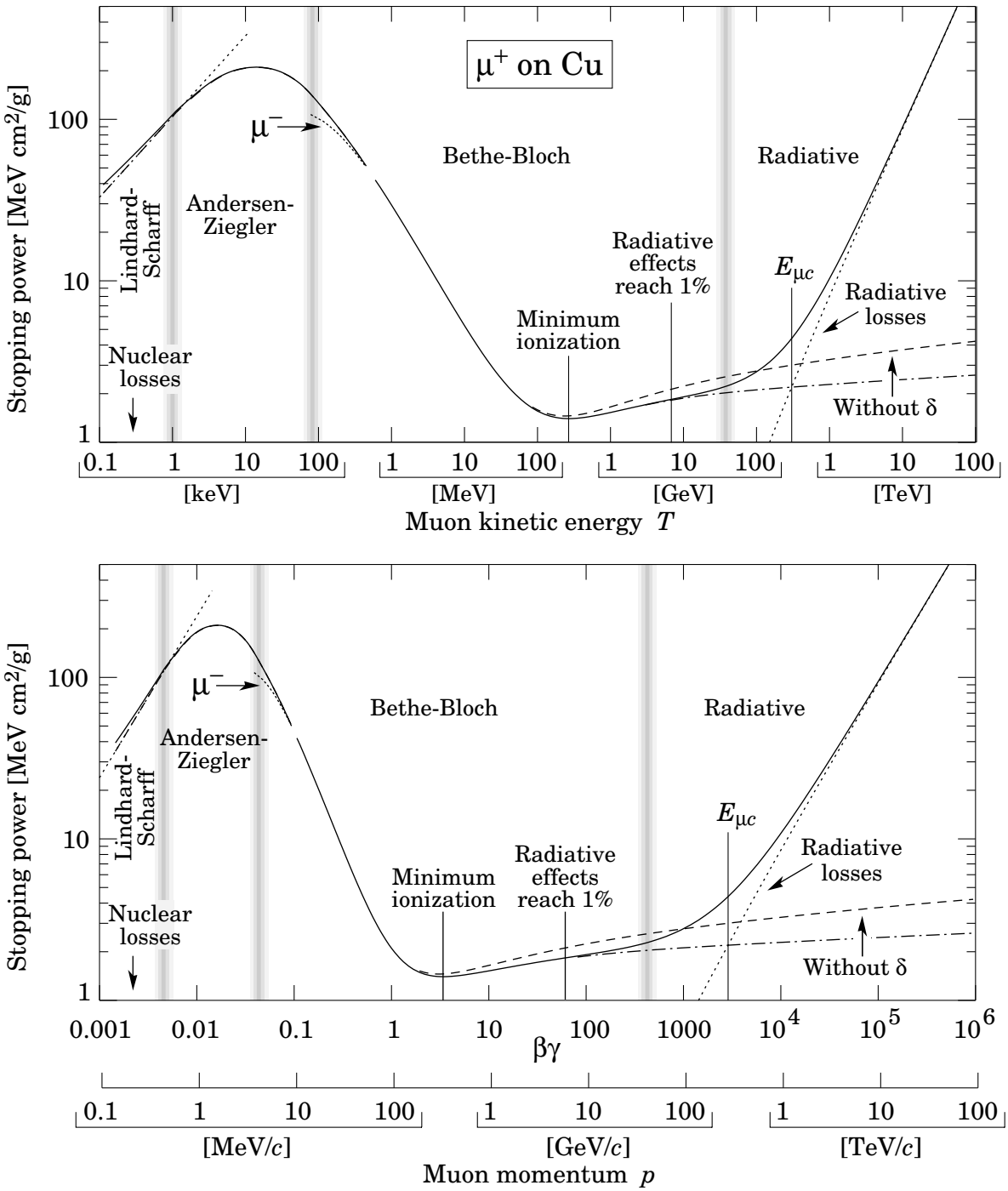

Figure 1: Stopping power ($= \langle -dE/dx \rangle$) for positive muons in copper as a function of kinetic energy T (top figure, 12 orders of magnitude range) and as a function of momentum $p = M\beta c\gamma$ (bottom figure, 9 orders of magnitude). Solid curves indicate the total stopping power. Data below the break at $T \approx 0.5$ MeV are scaled by the appropriate mass ratios from the π^- and p tables in ICRU 49 [3], and data at higher energies are from the present calculations. Vertical bands indicate boundaries between different theoretical approximations or dominant physical processes. The short dotted lines labeled "μ^-" illustrate the "Barkas effect" [8]. "Nuclear losses" indicates non-ionizing nuclear recoil energy losses, which are negligible here.

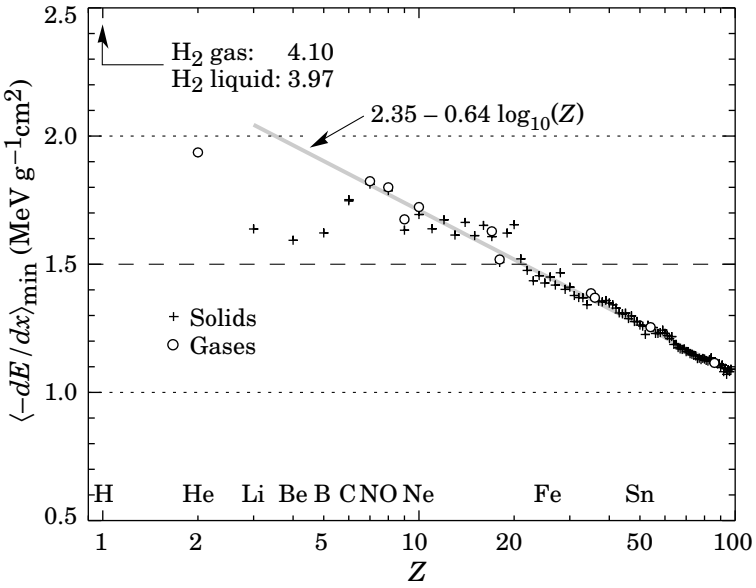

Figure 2: Minimum ionization as a function of Z. The straight line is fitted for $Z \geq 6$.

3. Electronic energy losses of high-energy heavy particles

The physics formulae needed to describe the average electronic energy losses of a high-energy ($\beta \gg \alpha Z$) massive ($\neq$ electron) charged particle as it passes through matter have been reviewed elsewhere [3, 16–24]. ICRU 49 is particularly useful, although it is limited to protons and alpha particles (except for a short π^- table) and to proton energies less than 10 GeV, corresponding to $E < 1.1$ GeV for muons. In this energy region nuclear recoil contributes negligibly to energy loss, and radiative losses, which typically become important above tens of GeV, and radiative losses can be added as an independent contribution.

For the moment, we leave open the possibilities that the charge is ze and that the particle might be something other than a muon. We briefly review the subject here in order to emphasize high-energy behavior.

3.1. Major contributions

The electronic stopping power[2] is calculated by summing the contributions of all possible inelastic scatterings. These are normally from lower to higher (bound or unbound) electronic energy states, so the particle loses a small amount of energy in each scattering. The kinetic energy of the scattered electron is Q.

In his derivation of the stopping power, Bethe [25] introduced the concept of "generalized oscillator strength" which is closely related to the inelastic-scattering form-factor [20]. The following summarizes the detailed discussions by Rossi [17], Fano [19], and Bichsel [24].

1. *Low-Q region.* Here the reciprocal of the 3-momentum transfer (roughly an impact parameter) is large compared with atomic dimensions. The scattered electrons have kinetic energies up to some cutoff Q_1, typically 0.01–0.1 eV [17]. For this region, Bethe approximated the generalized oscillator strength by the dipole oscillator strength $f(\varepsilon)$ which is the generalized oscillator

[2] Variously called S, $a(E)$, or the electronic part of the total mean energy loss rate $\langle -dE/dx \rangle$.

strength $f(\varepsilon, q)$ for zero momentum transfer q (ε is the energy loss in a single collision). $f(\varepsilon)$ is closely related to the optical absorption coefficient. He derived the following contribution to S:

$$S_{\rm low} = \frac{K}{2} z^2 \frac{Z}{A} \frac{1}{\beta^2} \left[\ln \frac{Q_1}{I^2/2m_e\beta^2c^2} + \ln \gamma^2 - \beta^2 \right] \tag{6}$$

Here $\ln I = \int f(\varepsilon) \ln \varepsilon \, d\varepsilon$. The denominator $I^2/2m_e\beta^2c^2$ in the first (logarithmic) term is the effective lower cutoff on the integral over dQ/Q. This term comes from "longitudinal excitations" (the ordinary Coulomb potential), and the next two terms from transverse excitations.

The low-Q region is associated with large impact parameters and hence with long distances. Polarization of the medium can seriously reduce this contribution, particularly at high energies where the transverse extension of the incident particle's electric field becomes substantial. The correction is usually made by subtracting a density-effect term δ, inside the square brackets of Eq. (6). This important correction is discussed in Sect. 3.4.

2. *Intermediate- and high-Q regions.* In an intermediate region atomic excitation energies are not necessarily small compared with Q, but transverse excitations can be neglected. At higher energies Q can be equated to the energy given to the electron, neglecting its binding energy. When the integration of the energy-weighted cross sections is carried out from Q_1 to some upper limit $Q_{\rm upper}$, one obtains

$$S_{\rm high} = \frac{K}{2} z^2 \frac{Z}{A} \frac{1}{\beta^2} \left[\ln \frac{Q_{\rm upper}}{Q_1} - \beta^2 \frac{Q_{\rm upper}}{Q_{\rm max}} \right] \ . \tag{7}$$

Here $Q_{\rm max}$ is the kinematic maximum possible electron recoil kinetic energy, given by

$$Q_{\rm max} = \frac{2m_e c^2 \beta^2 \gamma^2}{1 + 2\gamma m_e/M + (m_e/M)^2} \ . \tag{8}$$

$Q_{\rm upper}$ is normally equal to $Q_{\rm max}$ (as will be the case after the conclusion of this section), and cannot exceed $Q_{\rm max}$. The more general form given in Eq. (7) is useful in considering restricted energy loss, which is of relevance in considering the energy actually deposited in a thin absorber. At high energies (such that $Q_{\rm upper}/Q_{\rm max} \ll 1$) the first term in the square brackets dominates. If $Q_{\rm upper}$ is restricted to some maximum value, e.g. 0.5 MeV, then $S_{\rm high}$ is essentially constant for $Q_{\rm max} > Q_{\rm upper}$. If $Q_{\rm upper} = Q_{\rm max}$ the high-Q region stopping power rises with energy as $\ln Q_{\rm max}$. In other words, the increase of $S_{\rm high}$ with energy is associated with the production of high-energy recoil electrons, or δ-rays.

A very small projectile mass dependence of the electronic stopping power is introduced by $Q_{\rm max}$, which otherwise depends only on projectile velocity.

In Fano's discussion the low-energy approximation $Q_{\rm max} \approx 2m_e c^2 \beta^2 \gamma^2 = 2m_e p^2/M^2$ is implicit. Accordingly, Eq. (7) is more closely related to Rossi's form (see his Eqns. 2.3.6 and 2.5.4). This low-energy approximation is made in many papers of the Bevatron era, but is in error by a factor of two for a muon with $T = 10.8$ GeV. Note that $Q_{\rm max} \to E$ at very high energies.

3.2. Mean excitation energy

"The determination of the mean excitation energy is the principal non-trivial task in the evaluation of the Bethe stopping-power formula" [26]. Recommended values have varied substantially with time. Estimates based on experimental stopping-power measurements for protons, deuterons, and alpha particles and on oscillator-strength distributions and dielectric-response functions were given in ICRU 37 [27]. These were retained in ICRU 49 [3], where a useful comparison with other results is given, and they are used in the EGS4 [28] electron/photon transport code. These values (scaled by $1/Z$) are shown in Fig. 3. The error estimates are from Table 2 in Ref. 26. As can be seen, $I/Z \simeq 10 \pm 1$ eV for elements heavier than sulphur.

The figure also shows Bichsel's more recent determination of I for selected heavy elements [29]. He estimates uncertainties from 1.5% to 5%; the 5% errors are shown. The change from the ICRU 37 values is less than 7% in all of the 19 cases except for samarium (7.5%), tungsten (7.5%), bismuth (9.3%) and thorium (9.5%). In addition, the mean excitation energy for liquid water has been more recently determined to be 79.7 ± 0.05 eV [31], significantly higher than the ICRU 37 value, 75.0 eV. This reference also gives mean excitation energies for a variety of biological materials of interest here. In addition, Leung has described further corrections to stopping power theory due to relativistic effects of the target electrons [32]. Such effects could increase the stopping power by as much as 2% for high-Z targets. Bichsel has observed that this would be equivalent to lowering the mean excitation energy values for high-Z materials by as much as 10%.

We are strongly motivated to use the ICRU 37 mean excitation energies because of the availability of density effect parameters based on these values [5], yet in many cases the more recent values are superior and should be used. To investigate the consequences of errors or changes in the mean excitation energies, we ran a version of our code in which I was increased by 10% and no other changes were made. In the $T_\mu = 10$–100 MeV region, the stopping power increased by somewhat over 1% for carbon and iron. For lead it decreased by 2.6%–1.4% over this energy range. Since we did not modify the density-effect parameters, in particular $\overline{C}$ (see Eq. (12)), there was a residual $\approx 0.4\%$ at high energies. The density-effect correction essentially replaces I by the plasma frequency $\hbar\omega_p$ for $p/M \gtrsim 1000$, so the stopping power is completely insensitive to I for $T \gtrsim 100$ GeV, or for the lower half of our stopping power tables. The range integral always has contributions from lower-energy parts, but these also become increasingly insignificant as the energy increases. We therefore feel justified in using the older data, for which dependable density-effect parameters are available.

3.3. Low-energy corrections

The distant-collision contribution to the stopping power given by Eq. (6) was obtained by Bethe [25] with the approximation that the velocities of atomic electrons are small compared with that of the projectile. More precisely, Bethe's approximation was to replace the generalized oscillator strength by the dipole oscillator strength $f(\varepsilon)$ in obtaining this result. This leads to correction terms [16] which are different for each atomic shell. The "shell correction" for the jth shell is represented by $-2C_j/Z$, so that an additional term $-C/Z = -\sum C_j/Z$ appears in the square brackets of Eq. (6). Other ways to calculate the shell correction are discussed in Ref. 3. Unfortunately, the algorithms are not easy for the non-expert to implement.

The shell correction is not important at the energies of interest in this report. For example, the stopping power correction is 0.3% for a 10 MeV muon in iron, and 3% in uranium. It falls rapidly with increasing energy. But even at intermediate energies it plays a role in "starting" the range integral. To investigate its importance, and to compare our results with the proton stopping power and range-energy tables in ICRU 49 [3], we have used the simple but long-obsolete analytic

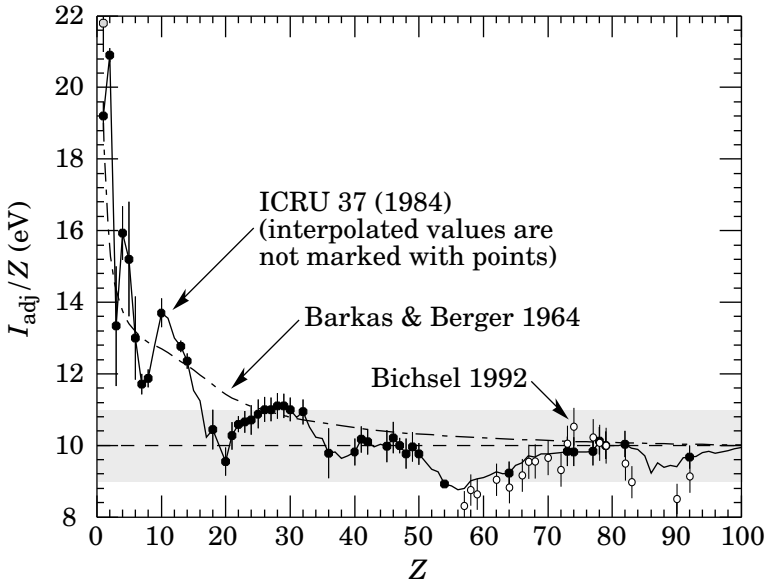

Figure 3: Mean excitation energies (divided by Z) as adopted in ICRU 37 [27] (filled points). Those based on experimental measurements are shown by symbols with error flags; the interpolated values are simply joined. The grey point is for liquid H_2; the black point at 19.2 is for H_2 gas. The open circles show more modern determinations by Bichsel [29]. The dotted curve is from the approximate formula of Barkas [30].

approximation for the shell correction introduced by Barkas [30]: [3] The accuracy of our results is addressed in Section 3.7.

In early Bevatron experiments Barkas et al. [8] found that negative pions had a somewhat greater range than positive pions with the same (small) initial energy. This was attributed to a departure from first-order Born theory [33], and is normally included by adding a term $zL_1(\beta)$ to the stopping-power formula. The effect has been measured for a number of negative/positive particle pairs, most recently for antiprotons/protons at the CERN LEAR facility [34]. It is illustrated by the μ^- stopping-power segment shown in Fig. 1.

Bethe's stopping power theory is based on a first-order Born approximation. To obtain Bloch's result, a term $z^2L_2(\beta)$ is added if results accurate at low energies are desired.

These corrections are discussed in detail in ICRU 49, and are mentioned here for completeness. They are not significant at the energies of concern in this report.

[3] Explicitly,

$$C = \left(0.422377\eta^{-2} + 0.0304043\eta^{-4} - 0.00038106\eta^{-6}\right) \times 10^{-6} I^2 + \left(3.858019\eta^{-2} - 0.1667989\eta^{-4} + 0.00157955\eta^{-6}\right) \times 10^{-9} I^3 \ , \quad (9)$$

where $\eta = \beta\gamma$ and I is in eV. This form is reasonably good only for $\eta > 0.13$ ($T = 7.9$ MeV for a proton, 0.89 MeV for a muon).

3.4. Density effect

As the particle energy increases its electric field flattens and extends, so that the distant-collision part of dE/dx (Eq. (6)) increases as $\ln\beta\gamma$. However, real media become polarized, limiting this extension and effectively truncating part of this logarithmic rise. This "density effect" has been extensively treated over the years; see Refs. 5, and 6, and 28, and references therein. The approach is to subtract a density-effect correction, δ, from the distant-collision contribution, resulting in the $\delta/2$ term in Eq. (15). At very high energies,

$$\delta/2 \to \ln\left(\hbar\omega_p/I\right) + \ln\beta\gamma - 1/2 \ , \tag{10}$$

where $\hbar\omega_p$ is the plasma energy defined in Table 1. As can be seen from Eq. (15), the effect of Eq. (10) is to replace I with $\hbar\omega_p$ and to eliminate the explicit $\beta^2\gamma^2$ dependence in the first (log) term in the square brackets. The remaining rise of the electronic stopping power comes from $Q_{\max}$, given by Eq. (8). The effect of the density correction is shown in Fig. 1.

At some low energy (related to x_0 below) the density effect is insignificant, and above some high energy (see x_1 below) it is well described by the asymptotic form given in Eq. (10). Conductors require special treatment at the low-energy end. Sternheimer has proposed the parameterization [35]

$$\delta = \begin{cases} 2\left(\ln 10\right)x - \overline{C} & \text{if } x \geq x_1; \\ 2\left(\ln 10\right)x - \overline{C} + a\left(x_1 - x\right)^k & \text{if } x_0 \leq x < x_1; \\ 0 & \text{if } x < x_0 \text{ (nonconductors);} \\ \delta_0 10^{2(x-x_0)} & \text{if } x < x_0 \text{ (conductors)} \ , \end{cases} \tag{11}$$

where $x = \log_{10}(p/M) = \log_{10}\beta\gamma$. $\overline{C}$ is obtained by equating the high-energy case of Eq. (11) with the limit of Eq. (10), so that

$$\overline{C} = 2\ln\left(I/\hbar\omega_p\right) + 1 \ . \tag{12}$$

The other parameters (a, k, x_0, x_1, and δ_0) are adjusted to give a best fit to the results of detailed numerical calculations for a logarithmically spaced grid of energy values. Note that $\overline{C}$ is the negative of the C used in earlier publications. A variety of different parameter sets are available. In some cases these result from a different fitting procedure having been used with the same model, and although the parameters look different the resulting δ is not sensibly different. For elements, the PEGS4 data [28] use the values from Ref. 36.

In a series of papers by Sternheimer, Seltzer, and Berger, the density-effect parameter tables are extended to nearly 300 elements, compounds, and mixtures. The chemical composition of the materials is given in Ref. 26.[4] The agreement with more detailed calculations or results obtained with other parameter sets is usually at the 0.5% level [37]; however, see Table IV in Ref. 38. We use the tables given in Ref. 5 for most of the present calculations.[5]

The densities used in these tables are occasionally in error, or, in the case of some polymers with variable density, out of the usual range. In this and other cases we use Eq. (A.8) [6] to adjust the parameters; these are marked by footnotes in the tables in Section 5.

[4] Slightly incorrect compositions (and therefore density effect parameters) are given for lanthanum oxysulfide (corrected in a footnote in Ref. 37), cellulose acetate, cellulose nitrate, polypropylene, and perhaps other materials. These will be corrected, and an approximately equal number of new materials added, in a forthcoming publication [39].

[5] Given the power of modern computers, experts now calculate the density effect from first principles rather than use these formulae [39]. One problem along the way is knowing the mean excitation energy, which can be different for condensed and gas states of the same substance and even depends upon density. In our case radiative effects dominate over most of the relevant energy range, and no great error is engendered by employing the user-friendly parameterized forms.

There remains the problem of obtaining the density-effect parameters if they have not been tabulated for the material of interest. This issue is of particular importance here in the case of cryogenic liquids such as N_2, but is also of interest when dealing with a compound or mixture not tabulated by Sternheimer, Berger, and Seltzer [5]. The algorithm proposed by Sternheimer and Peierls [6] is discussed in Appendix A.

To some degree, both the adjustment of the parameters for a different density and the Sternheimer–Peierls algorithm can be checked by using those cases in the tables where parameters are given for different densities of the same material. When the "compact carbon" parameters are adjusted to the two other tabulated carbon densities, the difference in stopping power and range with those obtained directly is less than 0.2%. Calculation of parameters for a cryogenic liquid using the Sternheimer-Peierls algorithm can be checked for hydrogen and water. This method was used to calculate parameters for liquid hydrogen at bubble chamber density (0.060 g/cm^3), using the excitation energy for the liquid; at worst, at minimum ionization, $\langle -dE/dx \rangle$ was low by 2.5%, while the range was high by 1.1%. Deviations were smaller elsewhere. When the algorithm was used to calculate parameters for water using the excitation energy for steam, the result was 1% higher at minimum ionization than that obtained directly with the water parameters. Only a slight improvement was obtained by using the excitation energy given for water.

Hydrogen is always a worst case. Sternheimer, Berger, and Seltzer [5] tabulate parameters for both hydrogen gas and liquid hydrogen under bubble chamber conditions, so we have made calculations in both directions via the Sternheimer-Peierls algorithm and by scaling densities via Eq. (*A.8*). We conclude that the stopping power results in this report obtained with parameters scaled to different densities are accurate to within the overall 0.5% agreement level estimated by Seltzer and Berger [37], and that the parameters calculated for cryogenic liquids (except hydrogen) using the Sternheimer-Peierls algorithm could produce stopping power errors of slightly over 1% at minimum ionization, and less elsewhere.

3.5. Other high-energy corrections

Bremsstrahlung from atomic electrons in the case of incident muons was considered in a 1997 paper by Kelner, Kokoulin, and Petrukhin [14]. There are four lowest-order diagrams: Photon emission by the muon before and after photon exchange with the electron, and emission by the electron before and after photon exchange. The former diagrams result in losses nearly proportional to E, and are described by Eq. (19). The latter are properly part of electronic losses, and produce an additional term in the stopping power. To leading powers in logarithms, this loss is given by:

$$\Delta \left| \frac{dE}{dx} \right| = \frac{K}{4\pi} \frac{Z}{A} \alpha \left[\ln \frac{2E}{M_\mu c^2} - \frac{1}{3} \ln \frac{2Q_{\max}}{m_e c^2} \right] \ln^2 \frac{2Q_{\max}}{m_e c^2} \tag{13}$$

As Kelner et al. observe, this addition is important at high energies, amounting to 2% of the electronic loss at 100 GeV and 4% at 1 TeV. It is included in our calculations.

An additional spin-correction term, $(1/4)(Q_{\max}/E)^2$, is included in the square brackets Eq. (7) if the incident particle is a muon (point-like and spin 1/2) [17]. Its contribution to the stopping power asymptotically approaches 0.038 (Z/A) MeV g^{-1}cm^2, reaching 90% of that value at 200 GeV in most materials. In iron its fractional contribution reaches a maximum of 0.75% at 670 GeV. Although this contribution is well within uncertainties in the total stopping power, its inclusion avoids a systematic bias.

At energies above a few hundred GeV, the maximum 4-momentum transfer to the electron can exceed 1 GeV/c, so that, in the case of incident pions, protons, and other hadrons, cross sections are modified by the extended charge distributions of the projectiles. One might expect this "soft"

cutoff to $Q_{\max}$ to reduce the electronic stopping power. This problem has been investigated by J. D. Jackson [15], who concluded that corrections to dE/dx become important only at energies where radiative losses dominate. At lower energies the stopping power is almost unchanged, since its average, dominated by losses due to many soft collisions, is insensitive to the rare hard collisions. For muons the spin correction replaces this form-factor correction.

Jackson and McCarthy [40] have pointed out that the Barkas correction calculated by Fermi (but see their Ref. 20) persists at high energies; hence, a term should be added to the close-collision part of Eq. (15):

$$Kz^3\frac{Z}{A}\frac{\pi\alpha}{2\beta} \tag{14}$$

This correction, which is ± 0.00176 MeV g^{-1} cm^2 for $z = \pm 1$, $Z/A = 1/2$ and $\beta = 1$, produces range differences of a few parts per thousand between positive and negative muons near minimum ionization. At higher energies sign-indifferent radiative effects dominate. We neglect this correction.

3.6. Bethe-Bloch equation

We summarize this discussion with the Bethe-Bloch equation for muons in the form used in this paper:

$$\left\langle -\frac{dE}{dx}\right\rangle_{\text{electronic}} = K\frac{Z}{A}\frac{1}{\beta^2}\left[\frac{1}{2}\ln\frac{2m_ec^2\beta^2\gamma^2Q_{\max}}{I^2} - \beta^2 - \frac{\delta}{2} + \frac{1}{8}\frac{Q^2_{\max}}{(\gamma Mc^2)^2}\right] + \Delta\left|\frac{dE}{dx}\right| \tag{15}$$

The final term, for bremsstrahlung from atomic electrons, is given by Eq. (13).

Except for the very small projectile mass dependence introduced by $Q_{\max}$, this expression depends only on the projectile velocity. This means that a value of the stopping power for a particle with mass M_1 and kinetic energy T_1 is the same as the stopping power for a particle with mass M_2 at $T_2 = (M_2/M_1)T_1$. Similarly, R/M is a function of T/M (or E/M, or p/M).

3.7. Comparison with other ionizing energy loss calculations

Comparisons with the ICRU 49 proton tables have been made by running our code with the proton mass. A summary of the stopping power comparisons is given in Table 2, and of the CSDA range comparisons in Table 3. In general the agreement is regarded as adequate, but is worse at high atomic number and low energy. The simple shell correction given by Eq. (9) has been used, and under these conditions somewhat overcorrects.

ICRU 49 concludes that the "differences between tabulated and experimental stopping powers are mostly smaller than 1% and hardly ever greater than 2%," and in the case of compounds and mixtures "the uncertainties are approximately three times as large as in the case of elements" [3].

Our muon tables start at $T = 10$ MeV, corresponding to a proton energy of about 100 MeV, so that only 100 MeV and above is relevant in the proton comparisons. For uranium the stopping power at 100 MeV is low by 0.8% and the range high by 1.9%. Without the shell correction the stopping power for this case is high by 1.7% and the range low by 2.5%. We make the shell correction only for elements. We conclude that in a worst-case scenario, $PuCl_4$ (which we do not tabulate) at 10 MeV, our results could be in error by nearly 3%. For lower-Z materials the agreement is consistent with ICRU 49. In any case the agreement improves rapidly with increasing energy.

Lohmann et al. [4] list muon electronic losses separately for hydrogen, iron, and uranium. Since they do not consider the contributions of bremsstrahlung from atomic electrons (Eq. (13)), we have made comparisons with this correction "turned off." Under these conditions, our results disagree

Table 2: Comparison of stopping power calculations for protons (in MeV g^{-1} cm^2) with those of ICRU 49 [3] and Bichsel 1992 [29].

	10 MeV	100 MeV	1 GeV	10 GeV
Hydrogen gas ($Z = 1$)				
This calculation	101.7	15.29	4.496	4.539
ICRU 49	101.9	15.30	4.497	4.539
Graphite ($Z = 6$, $\rho = 1.7$ g/cm^3)				
This calculation	40.72	6.514	1.942	1.883
ICRU 49	40.84	6.520	1.946	1.881
Iron ($Z = 26$)				
This calculation	28.54	5.045	1.575	1.603
ICRU 49	28.56	5.043	1.574	1.601
Tin ($Z = 50$)				
This calculation	22.26	4.177	1.351	1.426
ICRU 49	22.02	4.165	1.349	1.423
Lead ($Z = 82$)				
This calculation	17.52	3.532	1.189	1.291
ICRU 49	17.79	3.552	1.186	1.288
Bichsel 1992	17.79	3.592		
Uranium ($Z = 92$)				
This calculation	16.68	3.388	1.144	1.243
ICRU 49	16.90	3.411	1.140	1.242
Bichsel 1992	16.86	3.450		
Liquid water				
This calculation	45.94	7.290	2.210	2.132
ICRU 49	45.67	7.289	2.211	2.126

by at most 2 in the 4th decimal place, presumably from different rounding of the density-effect parameters.

4. Radiative losses

The radiative contribution to muon stopping power is conveniently written as $b(E)E$ [1], where $b(E)$ is a slowly-varying function of energy which is asymptotically constant. As indicated earlier, it is usually written as a sum of contributions from bremsstrahlung, direct pair production, and photonuclear interactions:

$$b \equiv b_{\rm brems} + b_{\rm pair} + b_{\rm nucl} \tag{2}$$

Here we describe the calculation of these contributions. Note that the convention $c = 1$ is used in all the formulae in this section.

In this section we specialize to $M = M_\mu$, although the results apply to any massive spin-1/2 pointlike particle. To a very rough approximation, the bremsstrahlung contribution scales as $1/M^2$, and the pair-production part as $1/M$. The results below probably apply fairly well to charged pion radiative energy losses, although to the best of our knowledge radiative losses by spin-0 particles has not been treated.

Table 3: Comparison of CSDA range calculations for protons (in g cm^{-2}) with those of ICRU 49.

	10 MeV	100 MeV	1 GeV	10 GeV
Hydrogen gas				
This calculation	0.0534	3.636	158.7	2254.
ICRU 49	0.0535	3.633	158.7	2254.
Graphite ($Z = 6,\ \rho = 1.7$ g/cm^3)				
This calculation	0.1361	8.634	367.4	5333.
ICRU 49	0.1377	8.627	367.0	5337.
Iron ($Z = 26$)				
This calculation	0.2013	11.36	459.2	6383.
ICRU 49	0.2064	11.37	459.6	6389.
Tin ($Z = 50$)				
This calculation	0.2623	13.90	540.9	7272.
ICRU 49	0.2764	13.95	541.9	7291.
Lead				
This calculation	0.3315	16.79	620.7	8120.
ICRU 49	0.3528	16.52	621.7	8143.
Uranium				
This calculation	0.3462	17.56	645.2	8432.
ICRU 49	0.3718	17.24	646.8	8456.
Liquid water				
This calculation	0.1201	7.710	325.4	4703.
ICRU 49	0.1230	7.718	325.4	4700.

4.1. Bremsstrahlung

The cross section for electron bremsstrahlung was obtained by Bethe and Heitler [41]. In the case of muons, it is necessary to take into account nuclear screening, which was first done consistently by Petrukhin and Shestakov [42]. A simple approximation for medium and heavy nuclei ($Z > 10$) was derived. Lohmann, Kopp, and Voss [4] also used this approximation, but for $Z < 10$ they set the nuclear screening correction equal to zero. As a result, their bremsstrahlung contribution for low-Z nuclei is overestimated by about 10%.

The CCFR collaboration [43] revised the Petrukhin and Shestakov [42] results, pointing out that Ref. 42 overestimates the nuclear screening correction by about 10%. Kelner et al. [44] later observed that the CCFR conclusion probably resulted from an incorrect treatment of the Bethe-Heitler formula. Their new calculations were in good agreement with the old ones by Petrukhin and Shestakov for medium and heavy nuclei, but in addition they proposed an approximation for light nuclei. An independent analysis was performed by the Bugaev group (see, e.g., Ref. 45). The results of Petrukhin and Shestakov and the Bugaev group for bremsstrahlung on screened nuclei agree to within a few percent.

All of the results mentioned above were derived in the Born approximation. It was recently shown [45] that the non-Born corrections in the region of low and high momentum transfers have the same order of magnitude but opposite signs. As a consequence, they nearly compensate each other.

The differential cross section for muon bremsstrahlung from a (screened) nucleus as given in Ref. 44 is used for the present paper:

$$\left.\frac{d\sigma}{d\nu}\right|_{\text{brems, nucl}} = \alpha \left(2Z\frac{m_e}{M_\mu}r_e\right)^2 \left(\frac{4}{3} - \frac{4}{3}\nu + \nu^2\right)\frac{\Phi(\delta)}{\nu} \tag{16}$$

Here ν is the fraction of the muon's energy transferred to the photon, and

$$\Phi(\delta) = \ln\left(\frac{BM_\mu Z^{-1/3}/m_e}{1+\delta\sqrt{e}\,BZ^{-1/3}/m_e}\right) - \Delta_n(\delta) \ , \tag{17}$$

where $D_n = 1.54A^{0.27}$, $B = 182.7$ ($B = 202.4$ for hydrogen), $e = 2.7181\ldots$, $\delta = M_\mu^2\nu/2E(1-\nu)$, and the nuclear screening correction Δ_n is given by

$$\Delta_n = \ln\left(\frac{D_n}{1+\delta\left(D_n\sqrt{e}-2\right)/M_\mu}\right). \tag{18}$$

The Thomas-Fermi potential for atomic electrons is assumed. A more precise calculation of the radiation logarithm using the Hartree-Fock model is described in Ref. 46, and the results agree with the Thomas-Fermi results within about 1% at high energies (total screening); the agreement is better at low energies. Since there is not yet a Hartree-Fock result for screening in the case of bremsstrahlung from atomic electrons, we prefer to use the form factors based on the Thomas-Fermi potential throughout.

To account for bremsstrahlung losses on atomic electrons, Z^2 in Eq. (16) is usually replaced with $Z(Z+1)$ (e.g., see Ref. 4). A much better approximation for the contribution from electrons, taking into account electronic binding and recoil, is given by [14]:

$$\left.\frac{d\sigma}{d\nu}\right|_{\text{brems, elec}} = \alpha Z \left(2\frac{m_e}{M_\mu}r_e\right)^2 \left(\frac{4}{3} - \frac{4}{3}\nu + \nu^2\right)\frac{\Phi_{in}(\delta)}{\nu} \tag{19}$$

In this case

$$\Phi_{in}(\delta) = \ln\left(\frac{M_\mu/\delta}{M_\mu\delta/m_e^2+\sqrt{e}}\right) - \ln\left(1+\frac{m_e}{\delta\,BZ^{-2/3}\sqrt{e}}\right) \ , \tag{20}$$

where $B = 1429$ for all elements but hydrogen, where $B = 446$, and $\delta = M^2\nu/2E(1-\nu)$, as above.

The cross section for bremsstrahlung as a function of fractional energy transfer ν is shown in Fig. 4. Although pair production dominates the radiative contributions to the stopping power, bremsstrahlung dominates at high ν.

The average energy loss $\langle -dE/dx\rangle$ due to bremsstrahlung is calculated by integrating the sum of these cross sections, as in Eq. (21) below.

4.2. Direct e^+e^- pair production

The cross section for direct e^+e^- pair production in a Coulomb field was first calculated by Racah [47]. Atomic screening was later taken into account by Kelner and Kotov [48]. With their approach, the average energy loss is obtained through a three-fold numerical integration. With the simple parameterization of the screening functions proposed by Kokoulin and Petrukhin [49], one obtains a double differential cross section for e^+e^- production. This formula is widely used in muon transport calculations (for example, see Ref. 4). Based on this work, a (rather complicated) analytic form for the energy spectrum of pairs created in screened muon-nucleus collisions was

derived by Nikishov [50]. The explicit formula is given in Appendix B. The average energy loss for pair production is calculated by numerical integration:

$$b_{\text{pair, nucl}} = -\frac{1}{E}\frac{dE}{dx}\bigg|_{\text{pair, nucl}} = \frac{N_A}{A}\int_0^1 \nu \frac{d\sigma}{d\nu} d\nu \tag{21}$$

The same expression as for the nucleus is usually used to calculate the pair production contribution from atomic electrons, with Z^2 replaced with Z (e.g., Ref. 4). A more precise approach has recently been developed by Kelner [51], who proposed a simple parameterization of the energy loss based on a rigorous QED calculation. This formula for the electronic contribution to pair production energy loss by muons is valid to within 5% of the more laborious numerical result for $E > 5$ GeV, and is used for the present calculations:

$$b_{\text{pair, elec}} = -\frac{1}{E}\frac{dE}{dx}\bigg|_{\text{pair, elec}} = \frac{Z}{A}\left(0.073\,\ln\left(\frac{2E/M_\mu}{1+g\,Z^{2/3}E/M_\mu}\right) - 0.31\right) \times 10^{-6}\text{cm}^2/\text{g} \tag{22}$$

Here $g = 4.4 \times 10^{-5}$ for hydrogen and $g = 1.95 \times 10^{-5}$ for other materials.

The cross section for direct pair production as a function of fractional energy transfer ν is shown in Fig. 4.

4.3. Photonuclear interactions

Several approaches have been developed to calculate the muon photonuclear cross section. The most widely used is that of Bezrukov and Bugaev [52]:

$$\begin{aligned}\frac{d\sigma}{d\nu}\bigg|_{\text{nucl}} = &\frac{\alpha}{2\pi} A\,\sigma_{\gamma N}(\varepsilon)\,\nu\left\{0.75\,G(x)\left[\kappa\,\ln\left(1+\frac{m_1^2}{t}\right) - \frac{\kappa m_1^2}{m_1^2+t} - \frac{2M_\mu^2}{t}\right]\right.\\ &+ 0.25\left[\kappa\,\ln\left(1+\frac{m_2^2}{t}\right) - \frac{2M_\mu^2}{t}\right]\\ &\left.+ \frac{M_\mu^2}{2t}\left[0.75\,G(x)\,\frac{m_1^2}{m_1^2+t} + 0.25\,\frac{m_2^2}{t}\,\ln\left(1+\frac{t}{m_2^2}\right)\right]\right\}\end{aligned} \tag{23}$$

Here ε is the energy loss of the muon and $\sigma_{\gamma N}(\varepsilon)$ is the photoabsorption cross section defined below. Other values are given by

$$\nu = \frac{\varepsilon}{E}\ ,\quad t = \frac{M_\mu^2\nu^2}{1-\nu}\ ,\quad \kappa = 1 - \frac{2}{\nu} + \frac{2}{\nu^2}\ ,\ \text{and}\ G(x) = \frac{3}{x^3}\left(\frac{x^2}{2} - 1 + e^{-x}(1+x)\right), \tag{24}$$

$x = 0.00282\,A^{1/3}\sigma_{\gamma N}(\varepsilon)$, $m_1^2 = 0.54$ GeV^2, and $m_2^2 = 1.8$ GeV^2. This cross section gives results consistent with other calculations to within 30% [4]. Recent measurements of photonuclear interaction of muon in rock performed by the MACRO collaboration [53] agree quite well with Monte Carlo simulations based on the Bezrukov and Bugaev cross section.

The total cross section $\sigma_{\gamma N}(\varepsilon)$ for the photon-nucleon interaction appears as a normalization parameter in Ref. 52, which proposes a simple parameterization:

$$\sigma_{\gamma N}(\varepsilon)\ \ (\text{in }\mu\text{b}) = 114.3 + 1.647\ln^2(0.0213\,\varepsilon) \tag{25}$$

This approximation is good enough only for muon energy loss $\varepsilon > 5$ GeV. For smaller ε, we use the experimental data given by Armstrong et al. [54]. The energy loss contribution is calculated by numerical integration of the differential cross section given by Eq. (23). The use here of a more precise photo-absorption cross section for $\varepsilon < 5$ than was used in the original model [52] does not change the photonuclear part of $\langle -dE/dx\rangle$ appreciably.

The cross section for photonuclear interactions as a function of fractional energy transfer ν is shown in Fig. 4.

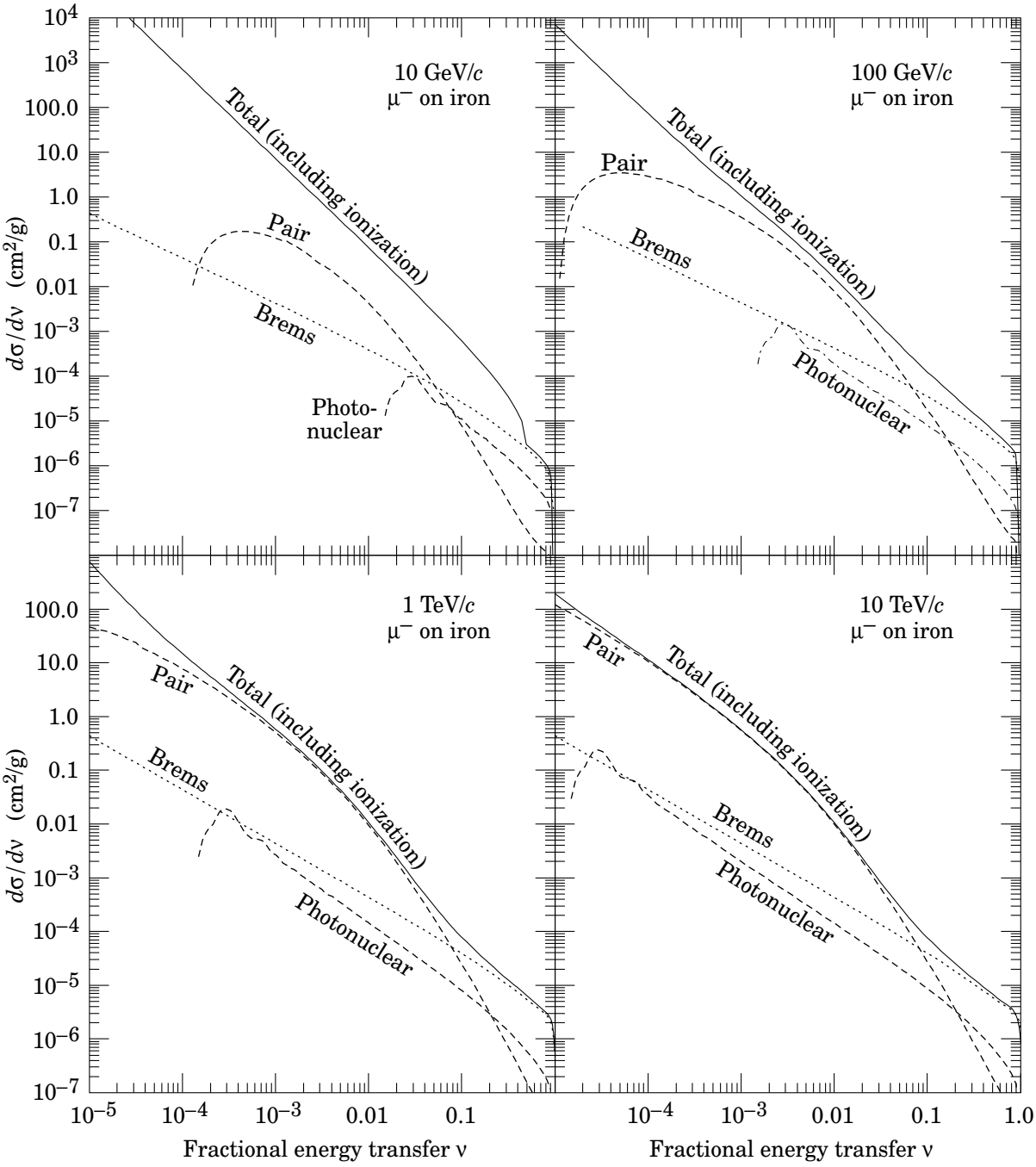

Figure 4: Differential cross section for total and radiative processes as a function of the fractional energy transfer for muons on iron.

Table 4: Comparison of $b_{\rm tot}$ calculations with those deduced from Lohmann et al. [4] and, in the case of standard rock, with Gaisser and Stanev [55]. $b_{\rm tot}$ is listed in units of $10^{-6}\,{\rm g}^{-1}\,{\rm cm}^2$.

Total energy =	10 GeV	100 GeV	1 TeV	10 TeV	100 TeV
Hydrogen					
This calculation	0.941	1.345	1.773	2.079	2.284
Lohmann *et al.*	1.081	1.463	1.814	2.046	—
Carbon					
This calculation	1.278	1.972	2.548	2.859	3.030
*Lohmann *et al.*	1.3	2.14	2.679	2.958	—
Iron					
This calculation	3.290	5.701	7.392	8.110	8.371
Lohmann *et al.*	3.312	5.795	7.444	8.128	—
Uranium					
This calculation	8.234	14.614	18.747	20.308	20.760
Lohmann *et al.*	8.046	14.790	18.870	20.360	—
Water					
This calculation	1.439	2.279	2.959	3.313	3.497
*Lohmann *et al.*	1.5	2.49	3.125	3.459	—
Standard rock					
This calculation	1.840	3.028	3.934	4.365	4.563
*Lohmann *et al.*	1.8	3.10	3.960	4.361	—
Gaisser & Stanev	1.91	3.12	4.01	4.40	—
Oxygen					
This calculation	1.502	2.397	3.108	3.468	3.650
*Lohmann *et al.*	1.6	2.62	3.290	3.620	—

* Obtained from the Lohmann et al. energy loss tables assuming our values for electronic losses (without the bremsstrahlung correction given by Eq. (13)). The subtraction loses significance at 10 GeV, where the radiative contribution is small.

4.4. Comparison with other works on muon radiative losses

Selected b values from our present calculations and according to Lohmann et al. [4] are listed in Table 4 and plotted in Fig. 5 as a function of muon energy. Since Lohmann et al. did not give the decomposition of the stopping powers except for H, Fe, and U, values of $b_{\rm tot}$ for the materials given in the right half of the figure were obtained by assuming our values of the ionizing losses (without the bremsstrahlung correction given by Eq. (13), which was omitted in Ref. 4). This is justified because for the fiducial cases H, Fe, and U our results agree with their values to within rounding errors in the 4th place.

For $Z > 10$ the results are nearly identical. For smaller atomic number, and at low energies, two effects are responsible for the differences:

1. In the nuclear part of bremsstrahlung, nuclear screening has only a weak energy dependence, and produces about a 4% reduction for hydrogen and a 10% reduction for carbon. This is apparent in our lower values of $b_{\rm tot}$ for carbon and water as compared with Lohmann et al.
2. The cross sections for bremsstrahlung and pair production from atomic electrons decrease at low energies because of electron recoil. In our calculations Lohmann et al.'s $Z(Z+1)$ factor is

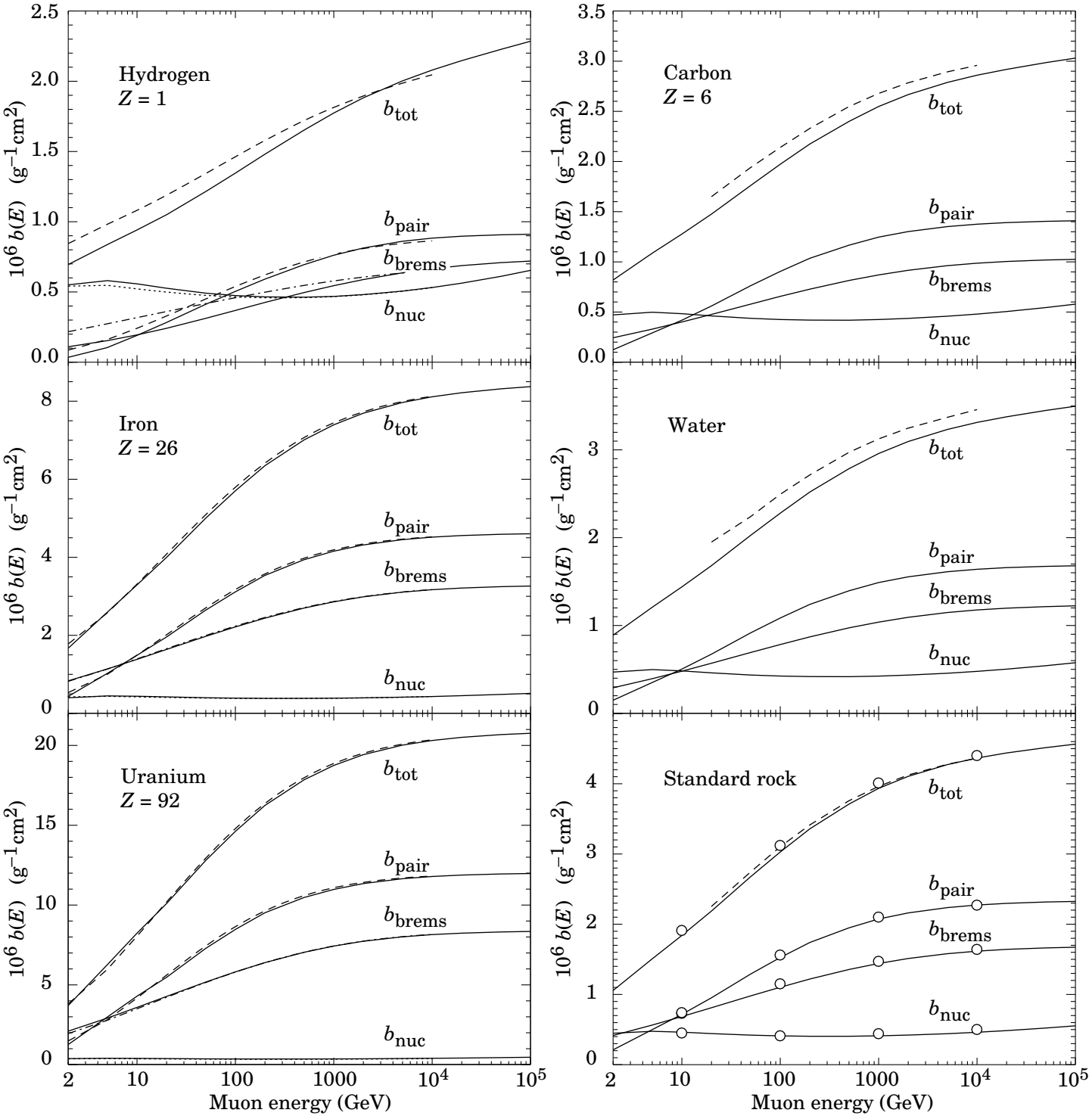

Figure 5: *b*-values for a sampling of materials. Solid lines represent our results, while the dashed/dotted lines are from Lohmann et al. [4]. The circles for standard rock are from Gaisser and Stanev [55].

replaced by $Z(Z+0)$ in the low-energy limit, so that for hydrogen our contributions to these processes for 1–10 GeV are smaller by nearly a factor of two. Similarly, in the low-energy limit our bremsstrahlung and pair production contributions for carbon are 6/7 of Lohmann et al.'s values.

The CERN RD 34 collaboration has measured the energy loss spectrum of 150 GeV muons in iron [56]. The energy deposition was measured in prototype hadron calorimeter modules for the ATLAS detector. Most probable electronic loss was subtracted, as was background from photonuclear interactions (which in this case is only about 7% of the total cross section). The remaining sensitivity was to energy loss by pair production (dominant at the smallest energy transfers, $0.01 < \nu < 0.03$), knock-on electrons (δ rays, included in the high-energy tail of the electronic loss and dominating for $0.03 < \nu < 0.12$), and bremsstrahlung (dominant for $\nu > 0.12$). The RD 34 experimental results shown in Fig. 6 are expressed as the fractional deviation from the present calculations, where the Kelner et al. [14] model (basically that of Petrukhin and Shestakov) is used to obtain the bremsstrahlung component important at large ν. The fractional deviations from our results are also shown for the CCFR collaboration's revision of the Petrukhin and Shestakov cross section [43] and Rozental's formula [57]. The present calculation describes the data reasonably well, while the others are evidently less successful.

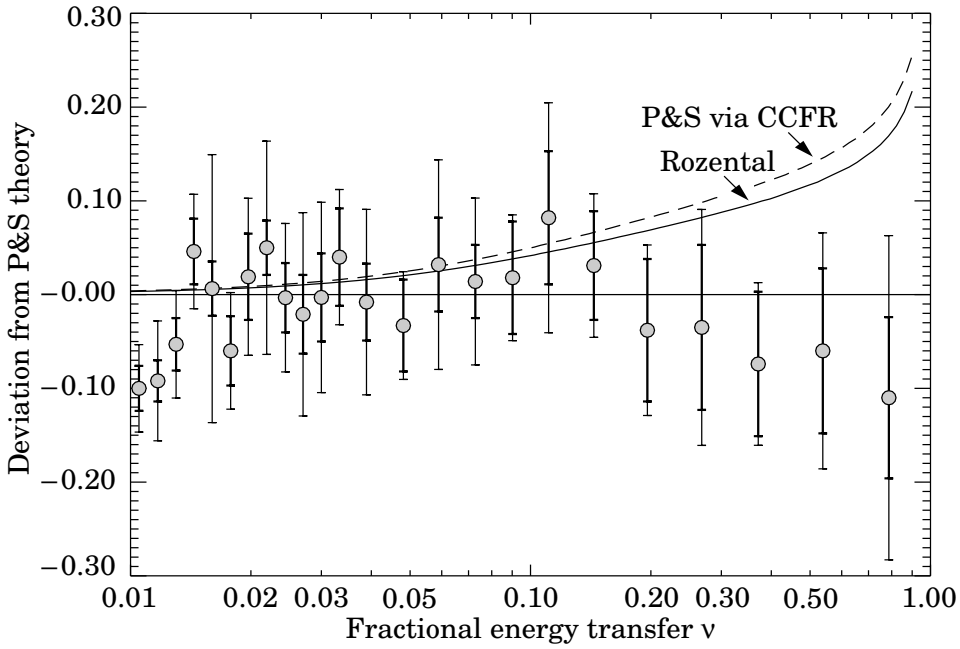

Figure 6: RD 34 measurements of energy losses by 150 GeV muons in iron [56], shown as fractional deviations from the present calculation, including bremsstrahlung via Kelner et al. [14]. Heavy error bars indicate statistical errors only, while the light bars include systematic errors combined in quadrature. Deviations of alternate models from our calculations are shown by the solid line (Rozental's formula [57]) and the dashed line (the CCFR collaboration's revision of the Petrukhin and Shestakov cross section [43]) .

4.5. Muon critical energy

Equation (5) defines the muon critical energy $E_{\mu c}$ as the energy for which electronic and radiative losses are equal. $E_{\mu c}$ for the chemical elements is shown in Fig. 7. The equality of electronic and radiative losses comes at a higher energy for gases than for solids and liquids because of the smaller density-effect correction for gases. Empirical functions have been fitted to these data for gases and for solids/liquids, in both cases excluding hydrogen from the fits. Since $E_{\mu c}$ depends upon ionization potentials and density-effect parameters as well as Z, the fits cannot be exact. Potassium, rubidium, and cesium are 3.6%, 3.2% and 3.4% high, respectively, while beryllium is 3.8% low. Most of the other solids and liquids fall within 2.5% of the fitted function. Among gases the worst fit is for neon (1.9% high).

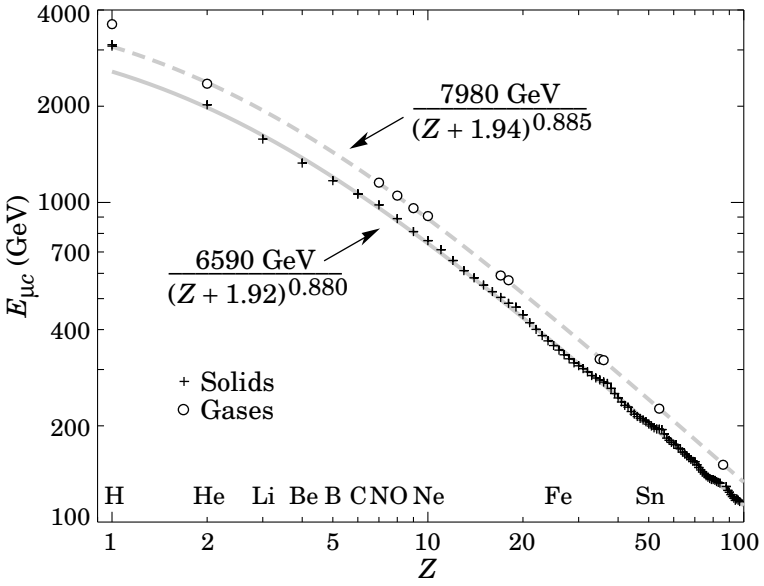

Figure 7: Muon critical energy for the chemical elements. As discussed in the text, the fitted functions shown in the figure cannot be exact, and are for guidance only.

4.6. Fluctuations in radiative energy loss

The radiative cross sections at several energies are shown in Fig. 4. The bremsstrahlung cross section varies roughly as $1/\nu$ over most of the range (where ν is the fraction of the muon's energy transferred in a collision), while for pair production the distribution varies as ν^{-3} to ν^{-2} (see also Ref. 58). "Hard" losses are therefore more probable in bremsstrahlung, and in fact energy losses due to pair production may very nearly be treated as continuous. The photonuclear cross section has almost the same shape as the bremsstrahlung cross section at high ν, but it is about an order of magnitude lower.

An example illustrating the fluctuations is shown in Fig. 8. The distribution of final muon momenta was obtained by following 10^5 1 TeV/c muons through 3 m (2360 g/cm^2) of iron, using the MARS14 Monte Carlo code [59]. Our result is in nearly exact agreement with results obtained earlier with TRAMU [58]. The most probable loss is 8 GeV, or 3.4 MeV g^{-1}cm^2. Our tables list a stopping power in iron as 9.82 MeV g^{-1}cm^2 for a 1 TeV muon, so that the mean loss should be 23 GeV, for a final energy ($\approx$ momentum $\times$ c) of 977 GeV, far below the peak. This is also the mean calculated from the simulated output.

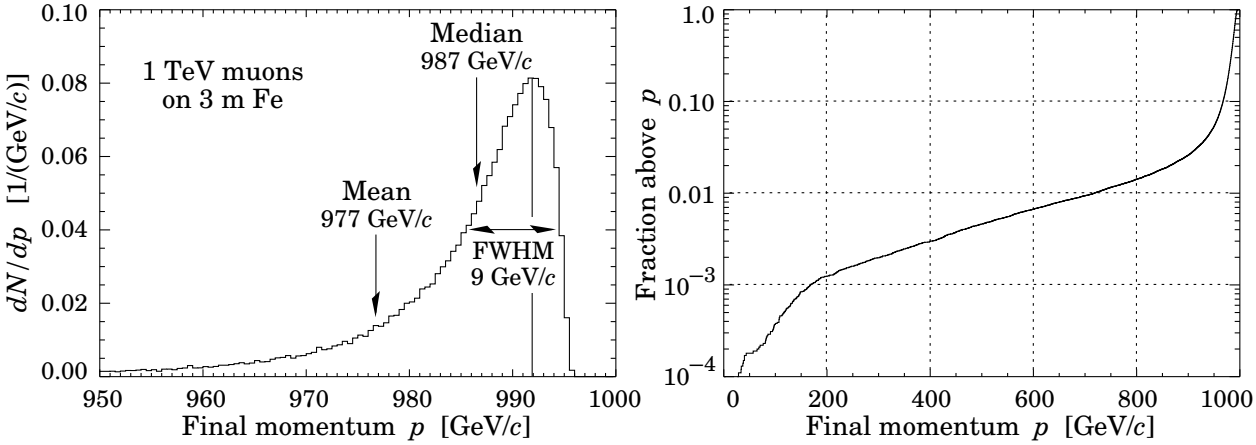

Figure 8: The momentum distribution of 1 TeV/c muons after traversing 3 m of iron, as obtained with the MARS14 Monte Carlo code [59]. The comparative rarity of very low final momenta follows from the approach of the cross sections to zero as $\nu \to 0$.

The full width at half maximum is 9 GeV/c, or 0.9%. The median is 988 GeV/c. 10% of the muons lost more than 3.2% of their energy and 2.6% lost more than 10% of their energy. Three out of the 10^5 candidates stopped in the iron, presumably because of very inelastic photonuclear interactions.

The classic case of the propagation of very high-energy muons in "standard rock" is discussed in Ref. 60 and references therein. Of special interest is Figure 3 of that paper, showing the survival probabilities as a function of depth for muons from 1 TeV to 10^6 TeV. The effects of the "radiative tail" are enormous; at 10^6 TeV only about 15% of the muons reach the CSDA range. At 10 TeV about half of them do, giving some indication of the usefulness of our CSDA ranges.

Treatment of radiative loss fluctuations in local energy deposit, range, or direction is beyond the scope of this paper. It is usually handled by Monte Carlo methods [58,60,61], although moment expansions are sometimes used when likelihoods need to be assigned to individual events. Electronic-loss straggling of high energy muons is described using a modified Vavilov distribution in Ref. 62.

5. Tabulated data

The contents of the main tables are shown in Tables 5–9. In this section we discuss the rationale in the selection of the elements, simple compounds, polymers, and biological materials for which tables of muon range-energy loss and radiative loss parameters are provided.

All "common" elements were selected. This included all elements with $Z \leq 38$ (strontium), most elements through $Z = 58$ (cerium), and the more common heavy elements through $Z = 94$ (plutonium). Dysprosium ($Z = 66$) was included to avoid a large gap in Z between cerium and tantalum ($Z = 73$). The list is given in Table 5.

Cryogenic liquid forms of most of the elemental room-temperature gases (radon is the exception) are fairly common in laboratories, and hence were included as well. Because of differences in the density effect corrections, ionization energy loss differ between liquid and gaseous forms. Radiative losses are not affected by density, but the muon critical energy, where the electronic and radiative losses are the same, can be quite different. We have excluded gaseous bromine, (boiling point

58.8° C, although it is tabulated by Sternheimer et al. [5]. For carbon, two forms with different densities appear. In all, 74 range/energy-loss tables are given for 63 elements

We should not overemphasize these differences: Related materials have similar stopping-power properties when these are listed in MeV cm^2/g (as we do) rather than in MeV/cm. Liquid and gaseous xenon are not dissimilar in spite of a density ratio of 540. Plutonium is more than twice as dense as bismuth, but their stopping powers differ by only 5% at minimum ionization. The stopping powers of hydrocarbons are quite similar, as are those of many polymers and biological materials.

Atomic weights are given to the available significance. This varies with element, since the isotopic composition of samples from different sources varies. In general the atomic weights of elements with only one isotope are known to great precision [63].

The same "commonness" criterion was applied to the selection of the simple compounds listed in Table 6, with some qualifications: We limited ourselves to the compounds listed by Sternheimer et al. [5], which meant that certain common compounds such as NaCl were not available. Common inorganic scintillators (BaF_2, BGO, CsI, LiF, LiI, NaI) are present. Materials such as trichloroethylene are included because of their role in important physics experiments. The list contains perhaps more hydrocarbons than necessary, in part to show the change of stopping power behavior as the H/C ratio changes (note the difference between acetylene and ethane). Liquid water and steam are both listed. Dry ice was included with some difficulty.

Polymers are listed in Table 7. Their energy loss behavior is quite similar except in the case of Teflon, which contains no hydrogen. "Thin film" polymers (Mylar, Kapton) were omitted. Polymers used for plastic scintillators (acrylic, polystyrene, polyvinyltolulene) are included. In some cases the name, like acrylic or polycarbonate, describes a family of polymers. The chemistry given is typical, and no great variation is to be expected except perhaps for "Bakelite," which is not very well characterized. Where space permits, the formula is given in such a way as to convey as much structural information as possible.

Mixtures of interest are given in Table 8. Muon energy loss in air is of great current interest, given atmospheric neutrino observations. Photographic emulsion is of more historic interest. Except for dry air (and, by definition, standard rock) none of the materials is particularly well characterized. The somewhat arbitrary concrete recipe is taken from *The Reactor Handbook* [64], and may be found, along with the other compositions, in Ref. 26.

For at least two generations, the depth of underground muon experiments has been reduced to depth in "standard rock." This is by definition the overburden of the Cayuga Rock Salt Mine near Ithaca, New York, where K. Greisen and collaborators made seminal observations of muons at substantial depths [1]. Ref. 1 says only "Most of the ground consists of shales of various types, with average density 2.65 g/cm^2 and average atomic number 11." Menon and Murthy later extended the definition: $\langle Z^2/A \rangle = 5.5$, $\langle Z/A \rangle = 0.5$, and and $\rho = 2.65$ g/cm^2 [65]. It was thus not-quite-sodium. Lohmann et al. [4] further assumed the mean excitation energy and density effect parameters were those of calcium carbonate, with no adjustments for the slight density difference. We use their definition for this most important material.

Sternheimer et al. [5] list 14 biological materials and "phantoms," mixtures which have nearly identical responses to radiation as the biological materials they replace. Omitted materials can be approximated by those on the list: Brain (ICRP), lung (ICRP), skin (ICRP), testes (ICRP), soft tissue (ICRU 4-component), and striated muscle (ICRU) are quite similar to soft tissue (ICRP), as are several included materials such as eye lens (ICRP) and skeletal muscle (ICRP). Compact bone (ICRU) is similar to cortical bone (ICRP).

Table 5: Index of tables for selected chemical elements. Physical states are indicated by "G" for gas, "D" for diatomic gas, "L" for liquid, and "S" for solid. Gases are evaluated at one atmosphere and 20° C. The corresponding cryogenic liquids are evaluated at their boiling points at one atmosphere, and carbon is evaluated at several typical densities. Atomic weights are given to their experimental significance. Except where noted, densities are as given by Sternheimer, Berger, and Seltzer [5].

Element	Symbol	Z	A	State	ρ [g/cm^3]	$\langle -dE/dx \rangle_{\rm min}$ [MeV cm^2/g]	$E_{\mu c}$ [GeV]	$\langle -dE/dx \rangle$ & Range	b	Notes
Hydrogen gas	H	1	1.00794	D	8.375×10^{-5}	4.103	3611.	I– 1	VI– 1	
Liquid hydrogen	H	1	1.00794	L	7.080×10^{-2}	4.034	3102.	I– 2	VI– 1	1
Helium gas	He	2	4.002602	G	1.663×10^{-4}	1.937	2351.	I– 3	VI– 2	
Liquid helium	He	2	4.002602	L	0.125	1.936	2020.	I– 4	VI– 2	2
Lithium	Li	3	6.941	S	0.534	1.639	1578.	I– 5	VI– 3	
Beryllium	Be	4	9.012182	S	1.848	1.595	1328.	I– 6	VI– 4	
Boron	B	5	10.811	S	2.370	1.623	1169.	I– 7	VI– 5	
Carbon (compact)	C	6	12.0107	S	2.265	1.745	1056.	I– 8	VI– 6	
Carbon (graphite)	C	6	12.0107	S	1.700	1.753	1065.	I– 9	VI– 6	
Nitrogen gas	N	7	14.00674	D	1.165×10^{-3}	1.825	1153.	I–10	VI– 7	
Liquid nitrogen	N	7	14.00674	L	0.807	1.813	982.	I–11	VI– 7	2
Oxygen gas	O	8	15.9994	D	1.332×10^{-3}	1.801	1050.	I–12	VI– 8	
Liquid oxygen	O	8	15.9994	L	1.141	1.788	890.	I–13	VI– 8	2
Fluorine gas	F	9	18.9984032	D	1.580×10^{-3}	1.676	959.	I–14	VI– 9	
Liquid fluorine	F	9	18.9984032	L	1.507	1.634	810.	I–15	VI– 9	2
Neon gas	Ne	10	20.1797	G	8.385×10^{-4}	1.724	906.	I–16	VI–10	
Liquid neon	Ne	10	20.1797	L	1.204	1.695	759.	I–17	VI–10	2
Sodium	Na	11	22.989770	S	0.971	1.639	711.	I–18	VI–11	
Magnesium	Mg	12	24.3050	S	1.740	1.674	658.	I–19	VI–12	
Aluminum	Al	13	26.981538	S	2.699	1.615	612.	I–20	VI–13	
Silicon	Si	14	28.0855	S	2.329	1.664	581.	I–21	VI–14	1
Phosphorus	P	15	30.973761	S	2.200	1.613	551.	I–22	VI–15	
Sulfur	S	16	32.066	S	2.000	1.652	526.	I–23	VI–16	
Chlorine gas	Cl	17	35.4527	D	2.995×10^{-3}	1.630	591.	I–24	VI–17	
Liquid chlorine	Cl	17	35.4527	L	1.574	1.608	504.	I–25	VI–17	2
Argon gas	Ar	18	39.948	G	1.662×10^{-3}	1.519	571.	I–26	VI–18	
Liquid argon	Ar	18	39.948	L	1.396	1.508	483.	I–27	VI–18	2
Potassium	K	19	39.0983	S	0.862	1.623	470.	I–28	VI–19	
Calcium	Ca	20	40.078	S	1.550	1.655	445.	I–29	VI–20	
Scandium	Sc	21	44.955910	S	2.989	1.522	420.	I–30	VI–21	
Titanium	Ti	22	47.867	S	4.540	1.477	401.	I–31	VI–22	
Vanadium	V	23	50.9415	S	6.110	1.436	383.	I–32	VI–23	
Chromium	Cr	24	51.9961	S	7.180	1.456	369.	I–33	VI–24	
Manganese	Mn	25	54.938049	S	7.440	1.428	357.	I–34	VI–25	
Iron	Fe	26	55.845	S	7.874	1.451	345.	I–35	VI–26	
Cobalt	Co	27	58.933200	S	8.900	1.419	334.	I–36	VI–27	
Nickel	Ni	28	58.6934	S	8.902	1.468	324.	I–37	VI–28	
Copper	Cu	29	63.546	S	8.960	1.403	315.	I–38	VI–29	
Zinc	Zn	30	65.39	S	7.133	1.411	308.	I–39	VI–30	
Gallium	Ga	31	69.723	S	5.904	1.379	302.	I–40	VI–31	
Germanium	Ge	32	72.61	S	5.323	1.370	295.	I–41	VI–32	

Table 5: continued

Element	Symbol	Z	A	State	ρ [g/cm^3]	$\langle -dE/dx\rangle_{\rm min}$ [MeV cm^2/g]	$E_{\mu c}$ [GeV]	$\langle -dE/dx\rangle$ & Range		b	Notes
Arsenic	As	33	74.92160	S	5.730	1.370	287.	I–42	VI–33		
Selenium	Se	34	78.96	S	4.500	1.343	282.	I–43	VI–34		
Bromine	Br	35	79.904	L	3.103	1.385	278.	I–44	VI–35		2
Krypton gas	Kr	36	83.80	G	3.478×10^{-3}	1.357	321.	I–45	VI–36		
Liquid krypton	Kr	36	83.80	L	2.418	1.357	274.	I–46	VI–36		2
Rubidium	Rb	37	85.4678	S	1.532	1.356	271.	I–47	VI–37		
Strontium	Sr	38	87.62	S	2.540	1.353	262.	I–48	VI–38		
Zirconium	Zr	40	91.224	S	6.506	1.349	244.	I–49	VI–39		
Niobium	Nb	41	92.90638	S	8.570	1.343	237.	I–50	VI–40		
Molybdenum	Mo	42	95.94	S	10.220	1.330	232.	I–51	VI–41		
Palladium	Pd	46	106.42	S	12.020	1.289	214.	I–52	VI–42		
Silver	Ag	47	107.8682	S	10.500	1.299	211.	I–53	VI–43		
Cadmium	Cd	48	112.411	S	8.650	1.277	208.	I–54	VI–44		
Indium	In	49	114.818	S	7.310	1.278	206.	I–55	VI–45		
Tin	Sn	50	118.710	S	7.310	1.263	202.	I–56	VI–46		
Antimony	Sb	51	121.760	S	6.691	1.259	200.	I–57	VI–47		
Iodine	I	53	126.90447	S	4.930	1.263	195.	I–58	VI–48		
Xenon gas	Xe	54	131.29	G	5.485×10^{-3}	1.255	226.	I–59	VI–49		
Liquid xenon	Xe	54	131.29	L	2.953	1.255	195.	I–60	VI–49		2
Cesium	Cs	55	132.90545	S	1.873	1.254	195.	I–61	VI–50		
Barium	Ba	56	137.327	S	3.500	1.231	189.	I–62	VI–51		
Cerium	Ce	58	140.116	S	6.657	1.234	180.	I–63	VI–52		
Dysprosium	Dy	66	162.50	S	8.550	1.175	161.	I–64	VI–53		
Tantalum	Ta	73	180.9479	S	16.654	1.149	145.	I–65	VI–54		
Tungsten	W	74	183.84	S	19.300	1.145	143.	I–66	VI–55		
Platinum	Pt	78	195.078	S	21.450	1.128	137.	I–67	VI–56		
Gold	Au	79	196.96655	S	19.320	1.134	136.	I–68	VI–57		
Mercury	Hg	80	200.59	L	13.546	1.130	136.	I–69	VI–58		
Lead	Pb	82	207.2	S	11.350	1.122	134.	I–70	VI–59		
Bismuth	Bi	83	208.98038	S	9.747	1.128	133.	I–71	VI–60		
Thorium	Th	90	232.0381	S	11.720	1.098	124.	I–72	VI–61		
Uranium	U	92	238.0289	S	18.950	1.081	120.	I–73	VI–62		
Plutonium	Pu	94	244.064197	S	19.840	1.071	117.	I–74	VI–63		

Notes:

1. Density effect parameters adjusted to this density using Eq. (*A.8*).
2. Density effect parameters calculated via the Sternheimer-Peierls algorithm discussed in Appendix A.

Table 6: Index of tables for selected simple compounds. Physical states are indicated by "G" for gas, "D" for diatomic gas, "L" for liquid, and "S" for solid. Gases are evaluated at one atmosphere and 20° C. Except where noted, densities are those given by Sternheimer, Berger, and Seltzer [5]. Composition not explained may be found in Seltzer and Berger [26] or in the file `properties.dat` at `http://pdg.lbl.gov/AtomicNuclearProperties`.

Compound or mixture	$\langle Z/A \rangle$	State	ρ [g/cm^3]	$\langle -dE/dx \rangle_{\rm min}$ [MeV cm^2/g]	$E_{\mu c}$ [GeV]	$\langle -dE/dx \rangle$ & Range	b	Notes
Acetone (CH_3CHCH_3)	0.55097	L	0.790	2.003	1160.	II– 1	VII– 1	
Acetylene (C_2H_2)	0.53768	G	1.097×10^{-3}	2.025	1400.	II– 2	VII– 2	
Aluminum oxide (Al_2O_3)	0.49038	S	3.970	1.647	705.	II– 3	VII– 3	
Barium fluoride (BaF_2)	0.42207	S	4.890	1.303	227.	II– 4	VII– 4	
Beryllium oxide (BeO)	0.47979	S	3.010	1.665	975.	II– 5	VII– 5	
Bismuth germanate (BGO, $Bi_4(GeO_4)_3$)	0.42065	S	7.130	1.251	176.	II– 6	VII– 6	
Butane (C_4H_{10})	0.59497	G	2.493×10^{-3}	2.278	1557.	II– 7	VII– 7	
Calcium carbonate ($CaCO_3$)	0.49955	S	2.800	1.686	630.	II– 8	VII– 8	
Calcium fluoride CaF_2	0.49670	S	3.180	1.655	564.	II– 9	VII– 9	
Calcium oxide (CaO)	0.49929	S	3.300	1.650	506.	II–10	VII–10	
Carbon dioxide (CO_2)	0.49989	G	1.842×10^{-3}	1.819	1094.	II–11	VII–11	
Solid carbon dioxide (dry ice)	0.49989	S	1.563	1.787	927.	II–12	VII–11	2
Cesium iodide (CsI)	0.41569	S	4.510	1.243	193.	II–13	VII–12	
Diethyl ether ($(CH_3CH_2)_2O$)	0.56663	L	0.714	2.072	1220.	II–14	VII–13	
Ethane (C_2H_6)	0.59861	G	1.253×10^{-3}	2.304	1603.	II–15	VII–14	
Ethanol (C_2H_5OH)	0.56437	L	0.789	2.054	1178.	II–16	VII–15	
Lithium fluoride (LiF)	0.46262	S	2.635	1.614	903.	II–17	VII–16	
Lithium iodide (LiI)	0.41939	S	3.494	1.272	207.	II–18	VII–17	
Methane (CH_4)	0.62334	G	6.672×10^{-4}	2.417	1715.	II–19	VII–18	
Octane (C_8H_{18})	0.57778	L	0.703	2.123	1312.	II–20	VII–19	
Paraffin ($CH_3(CH_2)_{n\approx 23}CH_3$)	0.57275	S	0.930	2.088	1287.	II–21	VII–20	
Plutonium dioxide (PuO_2)	0.40583	S	11.460	1.158	136.	II–22	VII–21	
Liquid propane (C_3H_8)	0.58962	L	0.493	2.198	1365.	II–23	VII–22	1
Silicon dioxide (fused quartz, SiO_2)	0.49930	S	2.200	1.699	708.	II–24	VII–23	1
Sodium iodide (NaI)	0.42697	S	3.667	1.305	223.	II–25	VII–24	
Toluene ($C_6H_5CH_3$)	0.54265	L	0.867	1.972	1203.	II–26	VII–25	
Trichloroethylene (C_2HCl_3)	0.48710	L	1.460	1.656	568.	II–27	VII–26	
Water (liquid) (H_2O)	0.55509	L	1.000	1.992	1032.	II–28	VII–27	
Water (vapor) (H_2O)	0.55509	G	7.562×10^{-4}	2.052	1231.	II–29	VII–27	

Notes:

1. Density effect parameters adjusted to this density using Eq. (A.8). Ref. 5 lists 2.32 g/cm^3 for SiO_2, which may be the density of cristobalite. The density of crystalline quartz is about 2.65 g/cm^3, and the density of fused quartz is typically 2.20 g/cm^3.
2. Density effect parameters calculated via the Sternheimer-Peierls algorithm discussed in Appendix A.

Table 7: Index of tables for selected high polymers. Except where noted, densities are those given by Sternheimer, Berger, and Seltzer [5]; actual densities of polymers will vary. Composition not explained may be found in Seltzer and Berger [26] or in the file `properties.dat` at `http://pdg.lbl.gov/AtomicNuclearProperties.`

Compound or mixture	$\langle Z/A\rangle$	ρ [g/cm^3]	$\langle -dE/dx\rangle_{\rm min}$ [MeV cm^2/g]	$E_{\mu c}$ [GeV]	$\langle -dE/dx\rangle$ & Range	b	Notes
Bakelite $[C_{43}H_{38}O_7]_n$	0.52792	1.250	1.889	1110.	III– 1	VIII– 1	
Nylon (type 6, 6/6) $[C_{12}H_{22}O_2N_2]_n$	0.54790	1.180	1.973	1156.	III– 2	VIII– 2	1
Polycarbonate $[OC_6H_4C(CH_3)_2C_6H_4OCO]_n$	0.52697	1.200	1.886	1104.	III– 3	VIII– 3	
Polyethylene $[C_2H_4]_n$	0.57034	0.890	2.079	1282.	III– 4	VIII– 4	1
Polymethylmethacrylate (acrylic)	0.53937	1.190	1.929	1107.	III– 5	VIII– 5	
Polystyrene $[C_6H_5CHCH_2]_n$	0.53768	1.060	1.936	1183.	III– 6	VIII– 6	
Polytetrafluoroethylene (Teflon) $[C_2F_4]_n$	0.47992	2.200	1.671	853.	III– 7	VIII– 7	
Polyvinylchloride (PVC) $[CH_2CHCl]_n$	0.51201	1.300	1.779	696.	III– 8	VIII– 8	
Polyvinyltoluene $[2\text{-}CH_3C_6H_4CHCH_2]_n$	0.54141	1.032	1.956	1194.	III– 9	VIII– 9	

Notes:

1. Density effect parameters adjusted to this density using Eq. (A.8).

Table 8: Index of tables for selected mixtures. Physical states are indicated by "G" for gas and "S" for solid. Gases are evaluated at one atmosphere and 20° C. Densities are those given by Sternheimer, Berger, and Seltzer [5]. Composition may be found in Seltzer and Berger [26] or in the file `properties.dat` at `http://pdg.lbl.gov/AtomicNuclearProperties.`

Compound or mixture	$\langle Z/A\rangle$	State	ρ [g/cm^3]	$\langle -dE/dx\rangle_{\rm min}$ [MeV cm^2/g]	$E_{\mu c}$ [GeV]	$\langle -dE/dx\rangle$ & Range	b
Air (dry, 1 atm)	0.49919	G	1.205×10^{-3}	1.815	1114.	IV– 1	IX– 1
Concrete	0.50274	S	2.300	1.711	700.	IV– 2	IX– 2
Lead glass	0.42101	S	6.220	1.255	175.	IV– 3	IX– 3
Photographic emulsion	0.43663	S	6.470	1.313	235.	IV– 4	IX– 4
Plate glass	0.49731	S	2.400	1.684	670.	IV– 5	IX– 5
Standard rock	0.50000	S	2.650	1.688	693.	IV– 6	IX– 6

Table 9: Index of tables for selected biological materials. Physical states are indicated by "L" for liquid and "S" for solid. Densities are those given by Sternheimer, Berger, and Seltzer [5]. Composition may be found in Seltzer and Berger [26] or in the file `properties.dat` at `http://pdg.lbl.gov/AtomicNuclearProperties.`

Biological material or phantom	$\langle Z/A \rangle$	State	ρ [g/cm^3]	$\langle -dE/dx \rangle_{\rm min}$ [MeV cm^2/g]	$E_{\mu c}$ [GeV]	$\langle -dE/dx \rangle$ & Range	b
A-150 tissue-equivalent plastic	0.54903	S	1.127	1.978	1158.	V– 1	X– 1
Adipose tissue (ICRP)	0.55947	S	0.920	2.029	1183.	V– 2	X– 2
Blood (ICRP)	0.54995	L	1.060	1.971	1032.	V– 3	X– 3
Cortical bone (ICRP)	0.52130	S	1.850	1.803	748.	V– 4	X– 4
C-552 air-equivalent plastic	0.49969	S	1.760	1.760	953.	V– 5	X– 5
Eye lens (ICRP)	0.54977	S	1.100	1.971	1057.	V– 6	X– 6
MS20 tissue substitute	0.53886	S	1.000	1.934	1056.	V– 7	X– 7
Skeletal muscle (ICRP)	0.54938	S	1.040	1.970	1032.	V– 8	X– 8
Soft tissue (ICRP)	0.55121	S	1.000	1.982	1063.	V– 9	X– 9

Acknowledgments

We wish to thank Felix Boehm (Caltech) for the invitation to write this report, and for his (and the editor's) gentle reminders and infinite patience while the work was in progress. Alberto Fassó (SLAC) was kind enough to make available his ASCII files of the density-effect coefficients and composition, vastly aiding verification of our parameters. Steve Seltzer (NIST) answered our questions and made available code which produced computer-readable files of the main tables of ICRU 49, making comparisons with our results much easier. Hans Bichsel, our "ghost author," first provided us with an exhaustive and supportive referee's report. This led to many changes and additions, including two new figures. Then, via conversations and email, further changes were made, and his suggested wording was used in parts of Sections 3.1 and 3.3. Finally, Bob Naumann (Dartmouth) carefully checked and corrected our structures for polymers. This work was supported by the U.S. Department of Energy under contract No. DE-AC03-76SF00098.

Appendix A. Stopping power and density-effect parameters for compounds and mixtures

For most of the materials for which tables are given in this report, the relevant effective excitation energy and density-effect parameters have already been tabulated, and should be used. This section concerns how to deal with an untabulated compound or mixture.

It is usual to think of a compound or mixture as made up of thin layers of the pure elements (or, better, constituent compounds for which tabulated data are available) in the right proportion (Bragg additivity [66]) . Let n_j be the number of the jth kind of atom in a compound (it need not be an integer for a mixture), and w_j its weight fraction:

$$w_j = n_j A_j \Big/ \sum_k n_k A_k \qquad A.1$$

Then

$$\left\langle \frac{dE}{dx} \right\rangle = \sum_j w_j \left. \frac{dE}{dx} \right|_j \qquad A.2$$

When the Bethe-Bloch equation is inserted and the radiative terms added, the Z-dependent terms can be sorted out to find that the mixture or compound is equivalent to a single material with

$$\begin{aligned} \left\langle \frac{Z}{A} \right\rangle &= \sum_j w_j \frac{Z_j}{A_j} &&= \sum_j n_j Z_j \Big/ \sum_j n_j A_j \\ \ln \langle I \rangle &= \sum_j w_j \left(Z_j/A_j\right) \ln I_j \Big/ \sum_j w_j \left(Z_j/A_j\right) &&= \sum_j n_j Z_j \ln I_j \Big/ \sum_j n_j Z_j \\ \langle b\left(E\right) \rangle &= \sum_j w_j b_j \left(E\right) \end{aligned} \qquad A.3$$

There are pitfalls in actually using Eq. (A.3) to calculate $\langle I \rangle$. Since the electrons in a compound are more tightly bound than in the constituent elements, the effective I_j are in general higher than those of the constituent elements. Exceptions are provided by diatomic gases and by metals in metallic alloys or compounds. Berger and Seltzer discuss ways to extend the Bragg additivity rule in lieu of a detailed calculation [26]:

(a) For a select list of materials (carbon and some common gases), they propose alternate mean excitation energies in their Table 5.1 (or Table 6 in Ref. 26).

(b) For other elements, the excitation energies are multiplied by 1.13 before calculation of the mean (the "13% rule"). Although it is is not said, it would seem sensible to apply this rule in the case of a tightly-bound material such as CsI, and not apply it in the case of a metallic compound like Nb_3Sn.

(c) Both are superseded by experimental numbers when available, as in the case of SiO_2.

Bragg additivity has little meaning in calculating the density-effect correction. If the material of interest is not available in the tables of Ref. 5, then the algorithm given by Sternheimer and Peierls [6] should be used. Their recipe is given more succinctly in the EGS4 manual [28], and the following algorithm is adopted from that version for the parameterization of Section 3.4.

(a) I is obtained as described above

(b) k is always taken as 3.00

(c) $\overline{C} = 2\ln(I/\hbar\omega_p) + 1$, with the plasma energy $\hbar\omega_p$ obtained using the expression from Table 1.

(d) For solids and liquids,

$$x_1 = \begin{cases} 2.0 & \text{if } I < 100 \text{ eV, and } x_0 = \begin{cases} 0.2 & \text{if } \overline{C} < 3.681 \\ 0.326\,\overline{C} - 1.0 & \text{otherwise} \end{cases} \\ 3.0 & \text{if } I \geq 100 \text{ eV, and } x_0 = \begin{cases} 0.2 & \text{if } \overline{C} < 5.215 \\ 0.326\,\overline{C} - 1.5 & \text{otherwise} \end{cases} \end{cases} \tag{A.4}$$

(e) In the case of gases,

$$x_0 = \begin{cases} 1.6 \text{ and } x_1 = 4.0 & \text{if } \overline{C} < 10.0 \\ 1.7 \text{ and } x_1 = 4.0 & \text{if } 10.0 \leq \overline{C} < 10.5 \\ 1.8 \text{ and } x_1 = 4.0 & \text{if } 10.5 \leq \overline{C} < 11.0 \\ 1.9 \text{ and } x_1 = 4.0 & \text{if } 11.0 \leq \overline{C} < 11.5 \\ 2.0 \text{ and } x_1 = 4.0 & \text{if } 11.5 \leq \overline{C} < 12.25 \\ 2.0 \text{ and } x_1 = 5.0 & \text{if } 12.25 \leq \overline{C} < 13.804 \\ 0.326\,\overline{C} - 1.5 \text{ and } x_1 = 5.0 & \text{if } \overline{C} \geq 13.804 \end{cases} \tag{A.5}$$

(f)

$$a = \frac{\overline{C} - 2\,(\ln 10)\,x_0}{(x_1 - x_0)^3} \ . \tag{A.6}$$

We have used this algorithm to calculate the density-effect coefficients for cryogenic liquids, which are not tabulated by Sternheimer, Berger, and Seltzer [5]. In this case, I for the gas was used.

One problem remains: Given the density-effect parameters, either from the literature [5] or from the algorithm given above, how does one modify them for the same material at a different density? This problem occurs for gases at different pressures, or for solid and liquids at different densities than those tabulated. In an early paper [6], Sternheimer noted that under quite general conditions

$$\delta_r\,(p) = \delta\,(p\sqrt{r}) \ , \tag{A.7}$$

where $r = \rho/\rho_0$, the ratio of desired to tabulated densities, and the subscript r indicates the quantity evaluated at the desired density. This implies [6] that

$$\begin{aligned} \overline{C}_r &= \overline{C} - \ln r \\ x_{0r} &= x_0 - \tfrac{1}{2}\log_{10} r \\ x_{1r} &= x_1 - \tfrac{1}{2}\log_{10} r \ . \end{aligned} \tag{A.8}$$

It is easily shown by matching different regions in Eq. (11) that the parameters a and k are unchanged by the transformation.

This method was used to correct the parameters for several materials for which we prefer different densities, for example the density of fused silica. Liquid hydrogen is tabulated for the "bubble chamber density," for which we scaled the parameters to the density of liquid hydrogen at its boiling point at a pressure of one atmosphere.

Both algorithms were checked by calculating $\langle -dE/dx \rangle$ several ways, taking advantage of the fact that Ref. 5 lists both gaseous and liquid helium, three densities of carbon, and both steam and liquid water. The comparisons are discussed at the end of Sect. 3.4.

Appendix B. Direct pair production from screened nuclei

Nikishov's analytic form for the cross section is given by [50]

$$\left.\frac{d\sigma}{d\nu}\right|_{\text{pair, nucl}} = \frac{(2\alpha r_e Z)^2}{\pi}\frac{(1-\nu)}{\nu}\left[(f_1+\theta f_3)\ln\left(\frac{2\varepsilon}{m_e}\right)+\phi_2+\theta\phi_4+I\right], \qquad B.1$$

where $\varepsilon=\nu E$ is the energy transferred to the e^+e^- pair, and $\theta=m_e^2/M^2$. The functions in the square brackets are given by

$$\begin{aligned} f_1+\theta f_3 = {} & \frac{44}{45z}-\frac{16}{45}-\frac{4}{9}\theta-\left(\frac{7}{9}+\frac{8}{45}z+\frac{7}{18}z\theta\right)\ln z \\ & +\left[\frac{16}{45}z+\frac{38}{45}-\frac{44}{45z}+\frac{4}{3(z+4)}+\left(\frac{7}{9}z-\frac{2}{9}+\frac{8}{3(z+4)}\right)\theta\right]B(z)\ln\frac{z_2}{z_1}\,, \end{aligned} \qquad B.2$$

$$\begin{aligned} \phi_2+\theta\phi_4 = {} & \left(\frac{7}{36}+\frac{2}{45}z+\frac{7}{72}z\theta\right)\left(\ln^2\frac{z_2}{z_1}+\pi^2+2\ln^2 z\right) \\ & +\left(\frac{7}{18}+\frac{3}{20}z+\frac{7}{36}z\theta\right)\ln z+\frac{653}{270}-\frac{28}{9z}+\frac{2}{3}\theta \\ & +\left[-\frac{3}{10}z-\frac{92}{45}+\frac{52}{45z}-\left(\frac{2}{9}-\frac{7}{18}z\right)\theta\right]B(z)\ln\frac{z_2}{z_1} \\ & +B(z)\left[-\frac{8}{45}z-\frac{19}{45}-\frac{8}{45z}-\left(\frac{2}{9}+\frac{7}{18}z\right)\theta\right]\left[\mathrm{Li}_2(y)+2\,\mathrm{Li}_2\left(\frac{1}{z_2}\right)+\frac{3}{2}\ln^2\frac{z_2}{z_1}\right] \\ & +\left(\frac{8}{z}+z\theta\right)\frac{B(z)}{3(z+4)}\times\left[6\,\mathrm{Li}_2\left(\frac{1}{z_2}\right)-\mathrm{Li}_2(y)+\frac{1}{2}\ln^2\frac{z_2}{z_1}\right]\,, \end{aligned} \qquad B.3$$

where

$$z=\frac{\nu^2}{\theta(1-\nu)},\quad z_{1,2}=B(z)\mp\frac{1}{2},\quad B(z)=\sqrt{\frac{1}{4}+\frac{1}{z}},\quad y=\frac{z_1+z_2}{z_2^2}\,,$$

Li_2 is the dilogarithm function (Spence's integral evaluated for $n=2$) [67], and

$$\begin{aligned} I = {} & \left(\frac{7}{9}+\frac{8}{45}z+\frac{7}{18}z\theta\right)H-\left[\frac{16}{45}z+\frac{38}{45}+\frac{16}{45z}+\left(\frac{7}{9}z+\frac{4}{9}\right)\theta\right]B(z)\,J_+ \\ & +\left[-\frac{16}{45}z-\frac{14}{9}-\frac{8}{9w}+\frac{2}{45}\frac{z}{w}-\frac{4}{5}\frac{z}{w^2}+\frac{2z}{3(w+4)}-\left(\frac{7}{9}z+\frac{4}{9}\frac{z}{w}\right)\theta\right]B(w)\,I_+ \\ & +\left[\frac{32}{45}\frac{u}{w}-\frac{88}{45z}-\frac{16}{45w}+\frac{8}{5}\frac{z}{w^2}+\frac{8}{9}\frac{u}{w}\theta\right]B(u)\ln\frac{u_2}{u_1} \\ & +\left[\frac{68}{45}-\frac{16}{45z}+\frac{8}{3w}-\frac{2}{3}\frac{z}{w}-\frac{8}{9}\theta\right]B(z)\ln\frac{z_2}{z_1}+\frac{104}{45z} \\ & -\frac{8}{15w}-\frac{62}{27}-\left(\frac{8}{9w}+\frac{1}{45}\frac{z}{w}+\frac{4}{5}\frac{z}{w^2}+\frac{4}{9}\frac{z}{w}\theta\right)\ln z \\ & +\left(1+\frac{1}{2}z\theta\right)\frac{1}{3w}\left(\ln^2\frac{u_2}{u_1}-\ln^2\frac{z_2}{z_1}\right) \\ & +\left(\frac{8}{z}+z\theta\right)\frac{B(z)}{3(z+4)}-\left[2J_+^{(2)}+\ln^2 z_2-\ln^2 z_1\right]\,, \end{aligned} \qquad B.4$$

where

$$\begin{aligned} & w=s\sqrt{z},\quad s=\frac{2\sqrt{\gamma\gamma'}Z^{1/3}}{183\sqrt{e}}\approx\frac{\sqrt{\gamma\gamma'}Z^{1/3}}{151}, \\ & u=w+z,\quad \gamma=P_0/M,\quad \gamma'=P_0'/M \end{aligned} \qquad B.5$$

($u_{1,2}$, $B(u)$ and $w_{1,2}$, $B(w)$ are the analogs of $z_{1,2}$, $B(z)$, i. e., $u_{1,2} = B(u) \mp \frac{1}{2}$, etc.),

$$\begin{aligned} H = {} & \mathrm{Li}_2\left(\frac{z}{u+4}\right) - \mathrm{Li}_2\left(\frac{z+4}{u+4}\right) + \mathrm{Li}_2\left(\frac{z}{z+4}\right) - 2\,\mathrm{Li}_2\left(\frac{u}{u+4}\right) \\ & + \mathrm{Li}_2\left(\frac{4w}{u\,(z+4)}\right) + \mathrm{Li}_2\left(\frac{4z}{u\,(w+4)}\right) - \mathrm{Li}_2\left(\frac{4}{w+4}\right) + \frac{\pi^2}{6} \\ & + 2\,\ln(z_1)\,\ln(z_2) - 4\,\ln(u_1)\,\ln(u_2) - \ln^2 z + \ln^2(z+4) - \ln\left(1+\frac{4}{w}\right)\ln(u+4) \\ & - \ln(4w)\,\ln(z+4) + \ln(16)\,\ln(u+4) - \ln^2(u+4) + 2\,\ln^2 u \\ & + \ln(u)\ln\left(\frac{z+4}{4}\frac{w+4}{4w}\right) - \ln(z)\,\ln\left(\frac{z+4}{4}\frac{u}{w}\right), \quad J_+ = J_+^{(1)} + J_+^{(2)}, \end{aligned} \tag{B.6}$$

$$J_+^{(1)} = 2\,\mathrm{Li}_2\left(\frac{1}{z_2}\right) - \mathrm{Li}_2(y) + \ln(z_1)\,\ln\frac{z_2}{z_1}, \quad y = \frac{z_1+z_2}{z_2^2}, \tag{B.7}$$

$$\begin{aligned} J_+^{(2)} = {} & \mathrm{Li}_2\left(\frac{u_1}{z_1}\right) - \mathrm{Li}_2\left(\frac{u_2}{z_2}\right) + \mathrm{Li}_2\left(\frac{z_1}{z_1+u_2}\right) - \mathrm{Li}_2\left(\frac{z_2}{z_2+u_1}\right) + \ln\left(\frac{u_1}{z_1}\right)\ln\left(1-\frac{u_1}{z_1}\right) \\ & - \ln\left(\frac{u_2}{z_2}\right)\ln\left(1-\frac{u_2}{z_2}\right) + \ln\left(\frac{z_2}{z_i}\right)\ln\left[u\,(z_1+u_2)\right] \ , \end{aligned} \tag{B.8}$$

and, finally,

$$\begin{aligned} I_+ = {} & \mathrm{Li}_2\left(\frac{u_1}{w_1}\right) - \mathrm{Li}_2\left(\frac{u_2}{w_2}\right) - 2\,\mathrm{Li}_2\left(\frac{w_1}{w_2}\right) + \mathrm{Li}_2\left(\frac{w_1}{w_1+u_2}\right) \\ & - \mathrm{Li}_2\left(\frac{w_2}{w_2+u_1}\right) + \frac{\pi^2}{3} + \ln\left(\frac{w_2}{w_1}\right)\ln\left(\frac{w_1+u_2}{w_2}\frac{u}{z}\right) \\ & + \ln\left(\frac{u_1}{w_1}\right)\ln\left(1-\frac{u_1}{w_1}\right) - \ln\left(\frac{u_2}{w_2}\right)\ln\left(1-\frac{u_2}{w_2}\right) \ . \end{aligned} \tag{B.9}$$

References

1. P. H. Barrett, L. M. Bollinger, G. Cocconi, Y. Eisenberg, and K. Greisen, Rev. Mod. Phys. **24**, 133 (1952).
2. R. M. Sternheimer, Phys. Rev. **117**, 485 (1960) 983–991 (1994).
3. "Stopping Powers and Ranges for Protons and Alpha Particles," ICRU Report No. 49 (1993); Tables and graphs of these data are available at `http://physics.nist.gov/PhysRefData/`.
4. W. Lohmann, R. Kopp, and R. Voss, "Energy Loss of Muons in the Energy Range 1–10000 GeV," CERN Report 85–03 (1985).
5. R. M. Sternheimer, M. J. Berger, and S. M. Seltzer, Atomic Data and Nuclear Data Tables **30**, 261–271 (1984).
6. R. M. Sternheimer and R. F. Peierls, Phys. Rev. **B3**, 3681–3692 (1971).
7. P. J. Mohr and B. N. Taylor, "CODATA Recommended Values of the Fundamental Physical Constants: 1998," J. Phys. Chem. Ref. Data **28**, 1713–1852 (1999).
8. W. H. Barkas, W. Birnbaum, and F. M. Smith, Phys. Rev. **101**, 778 (1956); H. Bichsel, Phys. Rev. **A41**, 3642–3647 (1990).
9. E. Fermi and E. Teller, Phys. Rev. **72**, 399–408 (1947).
10. J. Lindhard, Kgl. Danske Videnskab. Selskab, Mat.-Fys. Medd. **28**, No. 8 (1954); J. Lindhard, M. Scharff, and H. E. Schiøtt, Kgl. Danske Videnskab. Selskab, Mat.-Fys. Medd. **33**, No. 14 (1963).
11. T. Kaneko, Atomic Data and Nuclear Data Tables **53**, 271–283 (1993).
12. H. H. Andersen and J. F. Ziegler, *Hydrogen: Stopping Powers and Ranges in All Elements.* Vol. 3 of *The Stopping and Ranges of Ions in Matter* (Pergamon Press, 1977).
13. H. A. Bethe, "Quantenmechanic der Ein- und Zwei-Elektronen Probleme,' *Handbuch der Physik*, Vol. 24/1 (Springer-Berlin, 1933), p. 273.
14. S. R. Kelner, R. P. Kokoulin and A. A. Petrukhin, Phys. Atomic Nuclei **60**, 576–583 (1997) (Yad. Fiz. **60**, 657 (1997)).
15. J. D. Jackson, Phys. Rev. **D59**, 017301 (1999).
16. M. S. Livingston and H. A. Bethe, Rev. Mod. Phys. **9** 245–390 (1937); see especially pp. 261–276.
17. B. Rossi, *High Energy Particles*, (Prentice-Hall, Inc., Englewood Cliffs, NJ, 1952).
18. E. A. Uehling, Ann. Rev. Nucl. Sci. **4**, 315 (1954).
19. U. Fano, Ann. Rev. Nucl. Sci. **13**, 1 (1963).
20. M. Inokuti, Rev. Mod. Phys. **43**, 297 (1971).
21. H. Bichsel, in *American Institute of Phyics Handbook*, 3rd ed., edited by E. D. Gray (McGraw-Hill, New York, 1972), section 8d.
22. J. D. Jackson, *Classical Electrodynamics*, 2nd ed. (John Wiley & Sons, New York, 1975).
23. S. P Ahlen, Rev. Mod. Phys. **52**, 121 (1980).

24. H. Bichsel, in *Atomic, Molecular, and Optical Physics Handbook*, edited by G. Drake, (Am. Inst. Phys., 1996), Chap. 87.
25. H. Bethe, Ann. Phys. **5**, 325 (1930).
26. S. M. Seltzer and M. J. Berger, Int. J. Appl. Radiat. **33**, 1189–1218 (1982).
27. ICRU Report 37, "Stopping Powers for Electrons and Positrons," International Commission on Radiation Units and Measurements, Washington, DC (1984);
    Tables and graphs of these data are available at `http://physics.nist.gov/PhysRefData/`.
28. W.R. Nelson, H. Hirayama, and D. W. O. Rogers, "The EGS4 Code System," SLAC-265, Stanford Linear Accelerator Center (Dec. 1985).
29. H. Bichsel, Phys. Rev. **A46**, 5761 (1992).
30. W. H. Barkas and M. J. Berger, "Tables of Energy Losses and Ranges of Heavy Charged Particles," in *Studies in Penetration of Charged Particles in Matter*, National Academy of Sciences–National Research Council, Publication 1133 (1964), p. 103.
31. T. Hiraoka et al., Phys. Med. Biol. **39**, 983–991 (1994).
32. P. T. Leung, Phys. Rev. **A40**, 5417 (1989) 983–991 (1994).
33. W. H. Barkas, N. J. Dyer, and H. H. Heckmann, Phys. Rev. Lett. **11**, 26 (1963).
34. M. Agnello et al., Phys. Rev. Lett. **74**, 371 (1995).
35. R. M. Sternheimer, Phys. Rev. **88**, 851 (1952).
36. R. M. Sternheimer, S. M. Seltzer, and M. J. Berger, Phys. Rev. **B26**, 6067–6076 (1982).
37. S. M. Seltzer and M. J. Berger, Int. J. Appl. Radiat. **35**, 665–676 (1984). This paper corrects and extends the results of [26].
38. H. Bichsel, Rev. Mod. Phys. **60**, 663 (1960).
39. S. M. Seltzer, private communication.
40. J. D. Jackson and R. L. McCarthy, Phys. Rev. **B6**, 4131 (1972).
41. H. A. Bethe and W. Heitler, Proc. Roy. Soc. **A146**, 83 (1934);
    R. M. Sternheimer, S. M. Seltzer, and M. J. Berger, Phys. Rev. **B27**, 6971 (1983) (erratum).
42. A. V. Petrukhin and V. V. Shestakov, Can. J. Phys. **46**, S337 (1968).
43. W. K. Sakumoto et al., Phys. Rev. **D45**, 3042 (1992).
44. S. R. Kelner, R. P. Kokoulin and A. A. Petrukhin, preprint MSEPI 024-95, Moscow (1995), available as CERN Preprint Server SCAN-9510048.
45. Y. M. Andreev and E. V. Bugaev, Phys. Rev. **D55**, 1233 (1997).
46. S. R. Kelner, R. P. Kokoulin and A. A. Petrukhin, Phys. Atomic Nuclei **62**, 1894–1898 (1999).
47. G. Racah, Nuovo Cim. **16**, 93 (1937).
48. S. R. Kelner and Yu. D. Kotov, Sov. Jour. Nucl. Phys. **7**, 237 (1968) (Yad. Phys. **7**, 360 (1968)).
49. R. P. Kokoulin and A. A. Petrukhin, Acta Physica Acad. Sci. Hung. 29 Suppl. **4**, 277 (1970).
50. A. I. Nikishov, Sov. J. Nucl. Phys. **27**, 677–691 (1978) ((Yad. Phys. **27**, 1281–1289 (1978)).

51. S. R. Kelner, Phys. Atomic Nuclei **61**, 448 (1998) (Yad. Phys. **61**, 511 (1998)).

52. L. B. Bezrukov and E. V. Bugaev, Sov. J. Nucl. Phys. **33** 635–643 (1981) (Yad. Phys. **33**, 1195–1207 (1981)).

53. E. Scapparone et al., Nucl. Phys. B, Proc. Suppl. **75A**, 397–400 (1999).

54. T. A. Armstrong et al., Phys. Rev. **D5**, 1640 (1972);
T. A. Armstrong et al., Nucl. Phys. **B41**, 445 (1972).

55. C. Caso et al., "Review of Particle Physics," Eur. Phys. J. **C3**, 1 (1998);
The values calculated in this paper are used in the 2000 revision of the Gaisser and Stanev review in D. E. Groom et al., "Review of Particle Physics," Eur. Phys. J. **C15**, 1 (2000);
See also `http://pdg.lbl.gov`.

56. E. Berger et al., Z. Phys. C73, 455–463(1997).

57. I. L. Rozental Sov. Phys. Uspekhi **11**, 49 (1968) (Usp. Phys. Nauk. **94**, 91 (1968)).

58. A. Van Ginneken, Nucl. Instrum. Methods **A251**, 21–39 (1986).

59. N.V. Mokhov, "The MARS Code System User's Guide," Fermilab-FN-628 (1995);
N. V. Mokhov, S. I. Striganov, A. Van Ginneken, S. G. Mashnik, A. J. Sierk, J.Ranft, in *Proc. of the Fourth Workshop on Simulating Accelerator Radiation Environments* (SARE-4), Knoxville, TN, September 14-16, 1998, pp. 87–99, Fermilab-Conf-98/379 (1998), nucl-th/9812038-v2-16-Dec-1998;
N. V. Mokhov, in *Proc. of ICRS-9 International Conference on Radiation Shielding*, (Tsukuba, Ibaraki, Japan, 1999), J. Nucl. Sci. Tech., **1** (2000), pp. 167–171, Fermilab-Conf-00/066 (2000);
`http://www-ap.fnal.gov/MARS/`.

60. P. Lipari and T. Stanev, Phys. Rev. **D44**, 3543 (1991).

61. S. I. Striganov, Nucl. Phys. B (Proc. Suppl.) **51A**, 172 (1996).

62. S. I. Striganov, Nucl. Instrum. Methods **A322**, 225–230 (1992).

63. Commission on Atomic Weights and Isotopic Abundances, Pure and Appl. Chem. **68**, 2339 (1996);
G. Audi and A. H. Wapstra, Nucl. Phys. **A565**, 1 (1993).

64. *The Reactor Handbook*, 2nd ed. edited by R. C. Weast, (Interscience, New York, 1960), Vol. 1.

65. M. G. K. Menon and P. V. Ramana Murthy, in *Progress In Elementary Particle and Cosmic Ray Physics*, (North Holland, Amsterdam, 1967), Vol. 9, 161–243.

66. W. H. Bragg and R. Kleeman, Philos. Mag. **10**, 318 (1905).

67. M. Abramowitz and I. A. Stegun, *Handbook of Mathematical Functions*, National Bureau of Standards Applied Mathematics Series, No. 55, (U. S. Gov. Printing Office, 1964). The dilogarithm (Spence's integral for $n = 2$) is given by Eq. 27.7.1. CERNLIB routine DDILOG is used to calculate the function.

Explanation of Tables[4]

TABLE I: Muon energy loss rate and CSDA range for selected chemical elements.
The contents of Table I and other information are given in Table 5.

The header defines the element and state, and gives the parameters used to calculate the electronic stopping power:

Z: Atomic number.

A: Atomic weight.

ρ: Density. Gas density is evaluated at 20° C.

I: Mean excitation energy.

a—δ_0: Sternheimer *et al.* density effect parameters, as introduced in Sect. 3.4 and Eq. (11).

The body of the table presents ionizing energy loss (Eq. (15)) and the components of radiative loss rate (see Eqs. (1) and (2), as well as CSDA range obtained by integrating the total (Eq. (3)), as a function of the muon's initial kinetic energy T. The spacing of the independent variable is fairly uniform on a logarithmic scale. The corresponding momentum p is also given. The table is interrupted to show the points at which minimum ionization and muon critical energy (Eq. (5)) occur.

A radiative loss field is left blank if the stopping power contribution is less than 0.0001.

TABLE II: Muon energy loss rate and CSDA range for simple compounds.
The contents of TABLE II and other information are given in Table 6. The format is identical with TABLE I, except that $\langle Z/A\rangle$ (Eq. (A.3)) replaces Z and A.

TABLE III: Muon energy loss rate and CSDA range for high polymers.
The contents of TABLE III and other information are given in Table 7. The format is identical with TABLE II.

TABLE IV: Muon energy loss rate and CSDA range for mixtures.
The contents of TABLE IV and other information are given in Table 8. The format is identical with TABLE II.

TABLE V: Muon energy loss rate and CSDA range for biological compounds.
The contents of TABLE V and other information are given in Table 9. The format is identical with TABLE I, except that $\langle Z/A\rangle$ (Eq. (A.3))) replaces Z and A.

TABLE VI: b values for the elements listed in Table I.
Interpolation in $\log E$ is used to generate the b values shown in TABLE I and for the ionizing loss calculations. The contents are listed in Table 5.

TABLE VII: b values for the compounds listed in TABLE II.
TABLE VII has the same format as TABLE III except that $\langle Z/A\rangle$ replaces Z and A. The contents are listed in Table 6.

TABLE VIII: b values for the high polymers listed in TABLE III.
TABLE VII has the same format as TABLE VII. The contents are listed in Table 7.

TABLE IX: b values for the mixtures listed in TABLE IV.
TABLE VII has the same format as TABLE VII. The contents are listed in Table 8.

TABLE X: b values for the biological compounds listed in TABLE V.
TABLE VII has the same format as TABLE VII. The contents are listed in Table 9.

[4] Computer-readable versions of these tables can be found at `http://pdg.lbl.gov/AtomicNuclearProperties`